# A modular field system ~~enabling cavity ring-down spectroscopy~~ for near-surface, vertical profiling of ~~in-situ vapor observations~~ the atmospheric composition in harsh environments ~~: The ISE-CUBE system~~using cavity ring-down spectroscopy

Andrew W. Seidl[1], Harald Sodemann[1], and Hans Christian Steen-Larsen[1]

[1]Geophysical Institute and Bjerknes Centre for Climate Research, University of Bergen, Norway

**Correspondence:** Andrew W. Seidl (andrew.seidl@uib.no)

**Abstract.** ~~Over the last two decades, cavity~~ Cavity ring-down spectroscopy (CRDS) has allowed for increasingly widespread, in-situ observations of trace gases~~in vapor~~, including the stable isotopic composition of water vapor. However, ~~in-situ observation~~ gathering observations in harsh environments ~~pose~~ still poses a particular challenge, ~~as these CRDS analyzers are designed for use in a conventional laboratory. As such, field deployments typically enclose the instrument in a "quasi-laboratory". These deployments often involve substantial logistical effort, in addition to potentially affecting the measurement site, such as impacting flow conditions around near-surface processes.~~ especially in regard to observing the small-scale exchanges taking place between surface and atmosphere, which can have a vertical structure. We have designed the ISE-CUBE system as a modular CRDS deployment system for ~~stable water isotope measurements, with a specific focus on observing near-surface processes~~profiling stable water isotopes in the lowermost level of the surface layer. We tested the system during a two-week field campaign during Feb-March 2020 in Ny-Ålesund, Svalbard, Norway, with ambient temperatures down to $-30\,°C$~~, and winds gusting over $20\,m\,s^{-1}$~~. The system functioned suitably throughout the campaign, with field periods exhibiting only a ~~minimal decrease~~ marginal increase in isotopic measurement ~~precision ($\delta^{18}O$: 0.06 ‰ & $\delta D$: 0.47 ‰)~~ uncertainty (30 %) as compared to optimal laboratory operation. Over the $2\,m$ profiling range, we have been able to measure and resolve gradients on the time and spatial scales needed in an Arctic environment. ~~Having proven itself in challenging arctic conditions, the ISE-CUBE system can be readily adapted to the particular needs of future stable water isotope researchers, wherever their research aims might take them.~~

## 1 Introduction

Understanding exchange processes between the atmosphere and surface is fundamental to constrain fluxes between ~~compartments~~ reservoirs in the Earth System. There exist substantial knowledge gaps on ~~the~~ these processes and their representation in models, especially at high latitudes and other cold environments ~~. In these regions, strong gradients form in the surface layer during stable stratification , and govern~~ (Wahl et al., 2021; Ritter et al., 2016). Near surface ($<2\,m$) gradients of scalars can be

strengthened significantly due to the stable stratification that often occurs in these regions (Jocher et al., 2012; Zeeman et al., 2015) , which ultimately govern the fluxes of trace gases such as methane, carbon dioxide, and water vapor.

In ~~particular,~~ cold regions in particular, where ice and snow are prevalent, the quantification of the evaporation and condensation flux of water vapor requires ~~further~~ multi-height, in-situ measurements. ~~Hereby~~In this regard, the stable isotope composition of the water vapor is a valuable asset, as quantified by the heavy isotopologues, $HD^{16}O$ (D=deuterium, $^2H$) and $H_2^{18}O$, as well as the rarer $H_2^{17}O$~~, is a valuable asset in disentangling water vapor of different origin and undergoing different processes. For example, in 1961, Craig used the stable water isotope (isotopologue) (SWI) composition of meteoric waters to establish the 8-to-1 linear relationship between $H_2^{18}O$ and $HD^{16}O$. Dansgaard (1964) took this relationship further and detailed how it can encapsulate both latitudinal and continental information of the precipitation collection site. Since then, SWIs have been used to identify moisture source origin (Kurita, 2011; Steen-Larsen et al., 2013), as well as to quantify mixing processes (Noone, 2012; Sodemann, 2017) in the atmosphere. Many of these and other SWI studies have only been made possible through advances in observational technology.~~ . Hereby, the relative abundances of the stable water isotopes (isotopologues) (SWIs) impart information about phase changes, and thus the exchange between different reservoirs of the hydrological cycle.

~~Over the last two decades or so, laser~~ Laser spectroscopy has enabled the continuous, high-resolution observation of the ~~SWI~~ SWI composition in ambient air (Galewsky et al., 2016). In cavity ring-down spectroscopy (CRDS), the sample is guided through a measurement cavity with highly precise pressure and temperature control, while measuring the decay of a laser pulse in the infrared (Crosson et al., 2002; Gupta et al., 2009). Since the spectrometers are designed for set-up in a laboratory and similarly controlled environments, the in-situ measurement ~~of small-scale processes and gradientsinvolve inlet lines with manifolds (Steen-Larsen et al., 2013, 2014a; Berkelhammer et al., 2016), in addition to~~ often relies on pre-existing ~~structures (Bonne et al., 2014; Galewsky et al., 2011) or tents (Steen-Larsen et al., 2013; Wahl et al., 2021)~~structures (Bonne et al., 2014; Galewsky et al., 2011) or tents (Steen-Larsen et al., 2013; Wahl et al., 2021).

At such pre-existing structures, water vapor isotopes are often continuously measured at one or several fixed-height inlets. Fixed height inlets must balance the number of lines with the robustness of their obtained gradient. Due to variations on many time scales, the inlet may not be at a height of interest for a particular measurement. In addition, over cold regions, turbulence in the surface layer often vanishes for extended periods (Mahrt, 2014), giving diffusional exchange processes a larger role. Due to kinetic fractionation of the SWIs, diffusional processes are particularly relevant for interpreting the measured water isotope signals in terms of surface properties (Thurnherr et al., 2021). While fixed-height manifold systems are only partially able to resolve near-surface gradients, assessing the surface exchanges requires detailed profiling of the structure.

The characteristically dry ambient air in the high latitudes, and thus low absolute moisture concentration, limits the analytical precision of SWI measurements. Wall effects on the tubing can potentially further degrade measurement quality (Massman and Ibrom, 2008 . Therefore, short, heated inlet lines limit potential interactions between water vapor and the inner walls of tubing. The use of short inlet lines also promotes a faster response of the CRDS analyzer, allowing for finer resolution of ambient signal variations in time and space. Munksgaard et al. (2011, 2012) applied a pragmatic approach, whereby the analyzer and accompanying equipment were housed inside a single plastic chest (on the order of $1\,m^3$ in size) to facilitate their shipboard study of sea-

water along the tropical northeastern Australian coast. ~~A~~ Despite the advantage of flexibility and low interference with the environment, a similar approach has not yet been attempted for the ~~in-situ~~ measurement of water vapor isotopes in the cold environmental conditions typical for high latitude winter.

Here we present a modular, in-situ ~~CRDS measurement~~ profiling system, termed the ISE-CUBEs, that adequately protects the CRDS analyzer from the harsh arctic environment ~~, especially at extreme sub-zero temperatures~~during profiling of the near-surface layer. The ISE-CUBE system primarily consists of a stack of weather-proof plastic cases ~~that are interconnected electrically and pneumatically for sample and ventilation air . With~~ interconnected for ambient air sample transmission. These cases have a footprint of less than $1\,\mathrm{m}^2$ and a total volume of less than $0.5\,\mathrm{m}^3$~~, the ISE-CUBEs can be rapidly deployed at different sites and is at least an order of magnitude smaller than conventional approaches~~. Attachment of a profiling sample arm allows for the detailed measurement of surface layer ~~gradients in the range of 0 to 2 m~~ profiles in a $2\,\mathrm{m}$ range above the surface. An additional expansion module allows for the collection of water vapor in a cold trap system for later laboratory analysis, including $\mathrm{H}_2^{17}\mathrm{O}$. After a detailed description of the design principle and construction of the ~~measurement~~ system, we evaluate its performance and the data quality based on measurements from a two-week field campaign at Ny-Ålesund, Svalbard, where the system encountered ~~strong winds and~~ severe cold temperatures.

## 2 Measurement system design

The general aim of the ISE-CUBE system design was to enable ground-based~~in-situ measurements~~ , near-surface profiles of the vapor isotope composition~~without the need for additional sheltering~~. Installation and operation should be unaffected by weather conditions, in particular ~~wind~~ in regard to temperature and precipitation. ~~Ambient deployment temperatures should have minimal effect on the instruments~~The entire system should also have minimal flow disturbance. Wall effects in the inlet should be minimized ~~, and condensation~~ with short tubing lengths. Condensation need be prevented, to avoid measurement artifacts from fractionation and smoothed signals from memory effects. ~~An inlet module should allow profiling of the surface layer with minimal flow disturbance.~~ The system should be able to accommodate a cryogenic trapping module to collect discrete vapor samples for subsequent laboratory analysis. Based on these requirements, we designed a modular system that in its core was based on waterproof plastic containers, enabling setup by a single operator. We first give an overview of the overall arrangement of the measurement system, before describing each module in more detail.

### 2.1 Overall measurement system setup

The main ~~modules~~ body of the ISE-CUBE system ~~consist~~ consists of a stack of the two primary modules (Analyzer and Pump modules), in addition to the Cold Trap expansion module; a list giving specifics of individual components can be found in Table A1 (~~and even more details~~ more details on system composition/construction can be found in the Supplemental Material). All three modules use the same plastic container (iM2875 Storm, Pelican Products Inc), allowing for stacking and fastening of the the ~~assembly~~stack, with a footprint of $0.38\,\mathrm{m}^2$ (see Figure 1). Each of the three modules is constantly ventilated with a $40\,\mathrm{m}^3\,\mathrm{h}^{-1}$ centrifugal fan. A plastic canvas can be placed over the stack for additional weather protection.

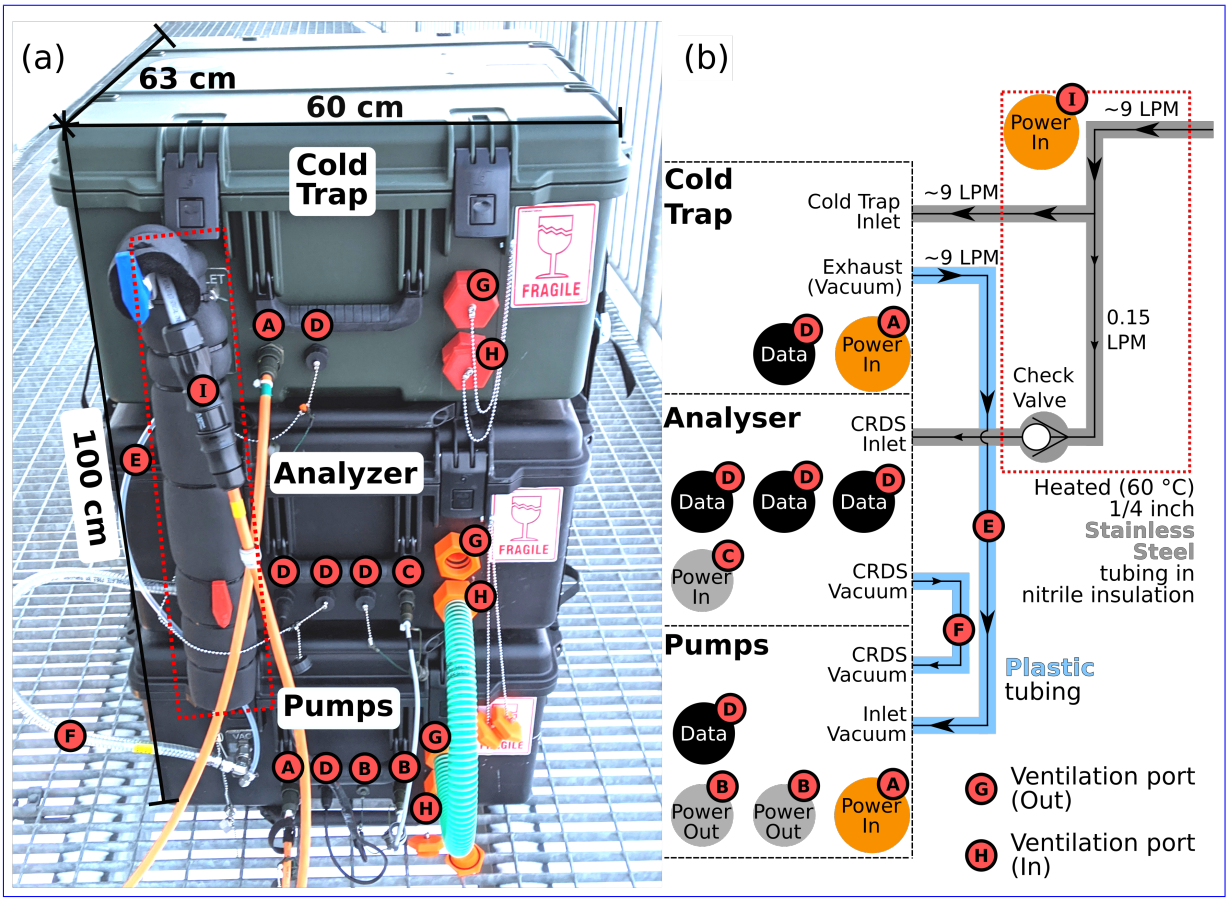


**Figure 1.** Overview of the ISE-CUBE system. (a) ISE-CUBEs in stacked configuration (from top to bottom): Cold Trap expansion module; Analyzer module; and Pump module. (b) Flow diagram for the entire ISE-CUBE system, including flow rates and connectors. A heated inlet assembly (red dotted area in both) ~~pneumatically~~ connects the three modules for common gas transmission. See text for details.

~~The stack is pneumatically interconnected~~ Gas transmission within the stack is via an inlet flow ~~adapter~~ assembly (Figure 1, red dotted area) composed of approximately $70\,\mathrm{cm}$ of $1/4\,\mathrm{inch}$ stainless steel tubing (Swagelok Inc.), heated to $60\,^{\circ}\mathrm{C}$ with self-regulating heat trace cabling (Thermon Inc.). A main flow of approximately $9\,\mathrm{L\,min^{-1}}$ is drawn into the ~~adapter~~ assembly (Figure 1b) with most going through the Cold Trapping module, using a vacuum pump in the Pump module (Figure 1b, "Inlet vacuum"). Analyzer flow is split off prior to entering the Cold Trapping module~~, and a~~. A one-way check valve upstream of the analyzer inlet bulkhead (Figure 1b, "Check Valve") prevents reversal of the flow of sample air bound for the analyzer. The external vacuum pump of the CRDS analyzer (N920AP.29.18, KNF DAC GmbH) is also located in the Pump module (Figure 1b, "CRDS vacuum"). The inlet flow ~~adapter~~ assembly also allows for connection to additional lengths of inlet tubing, such as the Profiling module which enables sampling at adjustable heights (see Sect. 2.4). We will now describe all four modules of the measurement system individually, beginning with the the Analyzer and Pump as the core modules.

### 2.2 Analyzer module

We use a Picarro CRDS water isotope analyzer (L2130-i, Picarro Inc., USA) as the central element of the Analyzer module (Figure 1, middle container). The Analyzer module is lined with custom-fit Low Density Polyethylene (LDPE) foam padding to protect the analyzer. Some padding can be removed to increase ventilation flow for better temperature regulation, depending on ambient conditions during field operations. With a power draw of $\sim$100 W in steady state there is substantial heating from the analyzer. Therefore, adequate ventilation is required to keep the analyzer internal temperatures ($T_{das}$) below ~~about~~ around 50 °C, as prolonged exposure to higher temperatures (above 70 °C) can permanently damage electrical components

The analyzer computer can be controlled from an external laptop through a ethernet (RJ45) cable, or via USB-connected monitor and keyboard/mouse combination, with the "Data" connectors (Figure 1, D). The particular analyzer used here (Ser#: HIDS2254) is a custom modification of the standard L2130-i, now enabled for high flow rates, similar to the analyzer described in Sodemann et al. (2017). The high flow rate is obtained by replacing the internal, constricting orifice (70 microns) needed for low-flow mode (typical flow rates $0.035\,\mathrm{L\,min^{-1}}$) with a standard $1/4$ inch stainless steel section, in addition to using a stronger vacuum pump (N920AP.29.18, KNF DAC GmbH, Germany). High flow rates (about $0.15\,\mathrm{L\,min^{-1}}$) enable faster analyzer response ~~, but~~ and 4 Hz sampling, but they also cause more variable pressure inside the measurement cavity. The full impact of this particular configuration will be discussed in more detail below (Sect. 4.1). Sample air is guided from the exterior inlet bulkhead of the module into the analyzer via a 20 cm piece of flexible, $1/4$ inch Polytetrafluoroethylene (PTFE) tubing. A similar length of $3/8$ inch, wire-reinforced, PVC tubing (K7160-06, Kuriyama of America Inc.) connects the vacuum port of the analyzer to the exterior bulkhead (Figure 1b, "CRDS Vacuum"). The vacuum and electrical bulkheads of the Analyzer module then connect to the Pump module (Figure 1, F: vacuum, B and C: electrical).

### 2.3 Pump module

The Pump module contains the pumps and additional components necessary for operation of the analyzer (Figure 1, bottom container). The Pump module is connected to the Analyzer module with a $3/8$ inch, wire-reinforced, PVC tubing (K7160-06, Kuriyama of America Inc.), providing the vacuum necessary for the analyzer (Figure 1b, "CRDS Vacuum"). The Inlet vacuum pump (N022AN.18, KNF DAC GmbH, Germany) continuously flushes the inlet tubing, providing the main flow for both the analyzer and the Cold Trapping module (see Sect. 2.5). Additionally, a small 300 W Uninterruptible Power Supply (UPS) (EL500FR, Eaton) inside the module protects the analyzer from possible power fluctuations and short power breaks. This UPS also provides 12 V power (via a 230 V AC-to-DC adaptor) for the Profiling module (Figure 1, B). All components in the Pump module are strapped to an aluminum support frame, which itself is firmly wedged between lid and bottom of the case, when the case is shut. Thereby, we could avoid drilling unnecessary mounting holes in the plastic case. Together, the Analyzer ~~Module~~ module and the Pump ~~Module~~ module are the two essential modules for in-situ isotopic ~~analysis~~ measurement of water vapor~~, and allow stand-alone field operation. The Cold Trapping module and the~~ . We will next describe how we can assign a spatial dimension to these measurements with the Profiling module.

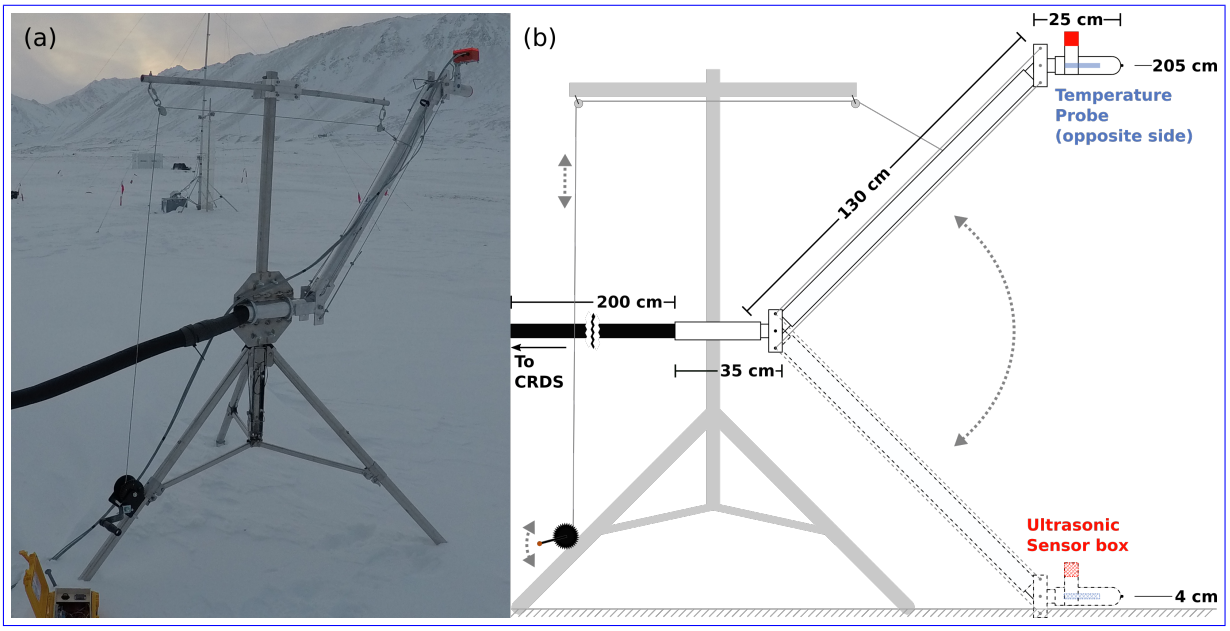


**Figure 2.** The Profiling module, with articulating arm. (a) Profiling module during field deployment. Inlet "head" in upper right of photo, with ultrasonic distance sensors encased in red plastic housing. Temperature sensor (not visible) located on opposite side of "head". Black winch in bottom left of photo controls inlet height via pulley system. Also visible in bottom left is the yellow case containing power supply and datalogger for temperature and distance sensors. Black tubing leading off to left connects to ISE-CUBE inlet. (b) Dimensional diagram for articulating arm.

### 2.4 Profiling module

The Profiling module allows us to measure near-surface gradients of water vapor (atmospheric composition, more generally), as well as to investigate the exchange processes between surface and atmosphere. The Profiling module ~~both expand upon the functionality of these core modules, as will be described next.~~ allows for the acquisition of vertical profiles of the ambient air at any height in a 2 m range (Figure 2). The lean design is expected to cause minimal flow disturbance at the measurement site. The module attaches to the inlet assembly (Figure 1, red dotted area) and consists of approximately 4 m of 1/4 inch stainless steel tubing (Swagelok Inc.), heated to 60 °C with self-regulating heat trace cable (Thermon Inc.), and surrounded with 2 cm thick foam nitrile insulation. Profiling capabilities are enabled by encasing the final 1.9 m of tubing in an aluminum articulating arm (Figure 2). The base of this arm is then attached to an aluminum mast and tripod with a custom-made steel mount (Supplemental material). The tripod serves as the frame for a winch and pulley system to manually control the sampling height (Figure 2). Additional environmental parameters are acquired during profiling from a sensor package mounted on the "head" of the arm, near the air inlet. Height of the inlet is monitored by ultrasonic distance sensors (HC-SR04, SparkFun Elec.; Figure 2, red box). Air temperature at inlet sampling height is measured using a temperature probe (VMA324, Velleman;

blue rectangle in Figure 2b). Both variables are logged onto an SD card via microcontroller (UNO, Arduino) housed inside a weatherproof container (Figure 2a, yellow case at lower left).

An alternate deployment frame was also custom-made for the profiling arm (see Supplemental Material; Figure S6). This allowed us to mount the arm on an elevated platform and to reach downwards to the surface of the water (such as at the Fjord deployment site, Sect. 3.1). The arm mounts onto a ladder-like construction with steel U-bolts. Two right-triangular steel supports are mounted on their base legs, perpendicular to the face of the ladder, forming the main structure of the frame. Base and height legs of the triangular supports are approximately 1 m long. A wheel-and-axle crossbeam connect the two supports at the upper point of the height leg; this crossbeam supports the steel cable moving the arm. Any rung of the ladder construction can slide into two steel brackets which are bolted to the platform. While in "normal" orientation, the ladder construction and the head of the inlet arm would be horizontal. However, the entire frame could then tip forwards, pivoting about the secured rung, with the ladder and inlet head both ending up vertical. This allowed us to make measurements 1.0 to 1.5 m further down at the Fjord site, though this did require an additional front-facing ultrasonic sensor. The fine-scale adjustment of the inlet head height was still possible with the winch and cable system, and was necessary to account for the tidal height changes of the seawater.

### 2.5 Cold Trapping expansion module

We included a cold trap module into the ISE-CUBE ~~assembly~~system, providing the ability to retrieve sample material from the field for subsequent laboratory analysis. ~~This discrete sample~~ This laboratory analysis could also ~~allow for calibration of the measurements if no external vapor source is available. In addition, more precise analyses, as are needed for~~ include $\delta^{17}$O for calculation of the $^{17}$~~O, can be performed in the laboratory afterwards~~O-excess. Many commercially available Cold Trapping options involve the use of liquid cooling agents, such as ethanol or isopropyl alcohol. Peters and Yakir (2010) demonstrated the feasibility of collecting vapor samples with a Stirling cycle cryocooler as the cryogenic source of a cold trap. Due to the safe transportation and fast installation of such a cold trap, we adopted the basic design of Peters and Yakir (2010) for the ISE-CUBE cold trap expansion module.

The cryocooler migrates heat away from the tip of a cryogenic "finger" towards the body of the cryocooler, where the heat is radiated away ~~.~~ through a radiator fin. By attaching this cryogenic finger to a thermally conducting mass (150 g of brass and aluminum) encircling a glass sampling vial, it directly cools the vial down to $-80\,^{\circ}\mathrm{C}$. Incoming water vapor in sample air (Figure 3b, "Inlet") is routed through a combination of $3/8$ inch stainless steel tubing and connectors, and is then introduced to the cooled glass collection vial, connected to the large bore tubing with a custom-made polycarbonate adapter ("PC" in Figure 3b). Upon entering the vial, the water vapor is rapidly cooled below its frost point, and it collects on the interior walls of the glass vial. The dried air exits the glass vial via a $1/8$ inch length of stainless steel tubing, leading out of the end of the $3/8$ inch tubing/connector combination. Finally, this $1/8$ inch tubing is connected to the Inlet vacuum pump (Figures 1b ~~&~~and 3b, "Exhaust (Vacuum)"), which provides the necessary flow for the Cold Trap. ~~The frozen sample is then sealed after the end of a sampling period , and~~ After the sampling period is complete, the flow is shut off with the needle valve

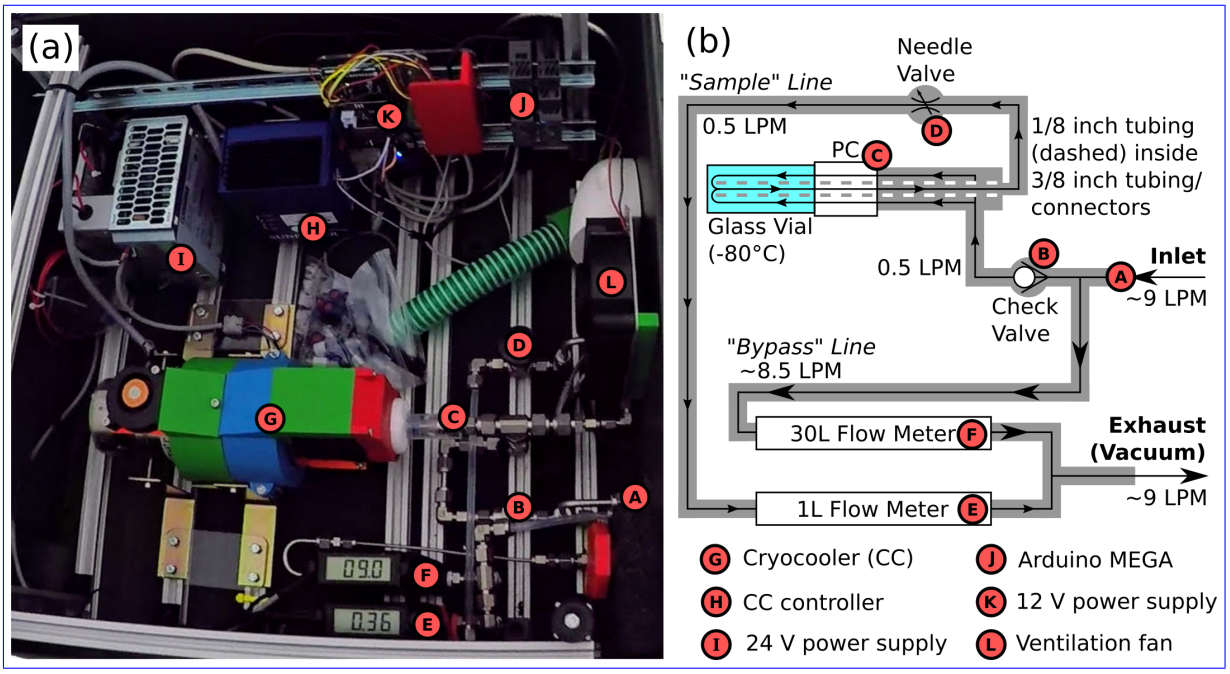


**Figure 3.** The Cold Trapping Module. (a) Interior of the module; cryocooler is surrounded by green, blue, and red plastic near photo center ("G"). (b) Flow diagram for the module. "PC" indicates placement of polycarbonate vial adapter. See text for details.

(Figure 3, D), and the vial is manually removed, sealed, and stored until laboratory analysis, which can be done from the same vial. Also, the relatively small size of the setup easily fits within the standard ISE-CUBE container (Figure 1, top box).

We modified the original design of Peters and Yakir (2010) with regard to two aspects, namely the choice of cryocooler, and the flow configuration. Firstly, we opted for a more powerful cryocooler (L. Peters, personal communication, 20 March 2019), enabling faster and more consistent cooling of the sampling vial. Our chosen cryocooler (~~Figure 3a, underneath red, green, and blue plastic casing,~~ Cryotel MT, Sunpower Inc.; Figure 3, G) takes 5 to 6 minutes to reach $-80\,^{\circ}\mathrm{C}$, at which temperature it has 23 W of cooling power. Secondly, as the system was designed to work in concert with the Analyzer and Pump modules, we utilized the Inlet pump described in Sect. 2.3 to provide flow through the collection vial. Accomplishing this required the splitting of flow inside the Cold Trapping module into a "sample" and "bypass" line (Figure 3b). The "sample" line allowed incoming, moist air into the glass collection vial, with flow regulation (approximately $0.5\,\mathrm{L\,min^{-1}}$ or less) via a manual needle valve. The "bypass" line carried the excess flow (approximately $8.5\,\mathrm{L\,min^{-1}}$), ensuring that the flushing of the inlet was maintained. Flow rates through the "sample" and "bypass" lines were monitored using $1\,\mathrm{L\,min^{-1}}$ and $30\,\mathrm{L\,min^{-1}}$ mass flow meters (TopTrak 822, Sierra Instruments Inc.; Figure 3, E and F), respectively. These flow meters recorded onto an SD card via microcontroller (Mega, Arduino; Figure 3, K), which in turn allowed for remote monitoring of the flow rates via the external USB bulkhead (Figure 1, D). Splitting the lines in such a way allowed the Inlet pump to provide flow through both the Cold Trap collection vial and the inlet tubing~~, which included the Profiling expansion module~~.

### 2.6 Profiling expansion module

To enable detailed investigation of near-surface gradients of water vapor, and exchange processes between surface and atmosphere, we designed a profiling expansion module for the ISE-CUBE system. The Profiling module allows for the acquisition of vertical profiles of the ambient vapor at any height between 4 to 205 cm above ground (Figure 2). Thereby, the lean design is expected to causes minimal flow disturbance at the measurement site. The module attaches to the inlet adapter and consists of approximately 4 m of 1/4 inch stainless steel tubing (Swagelok Inc.), heated to 60 °C with self-regulating heat trace cable (Thermon Inc.), and surrounded with 2 cm thick foam nitrile insulation. Profiling capabilities are enabled by an encasing of the final 1.9 m of tubing by an aluminum articulating arm (Figure 2). The base of this arm is then attached to an aluminum mast and tripod. The tripod serves as the frame for a winch and pulley system to manually control the sampling height (Figure 2). Additional environmental parameters are acquired during profiling from a sensor package mounted on the "head" of the arm, near the air inlet. Height of the inlet is monitored by ultrasonic distance sensors (HC-SR04, SparkFun Elec.; Figure 2, red box). Air temperature at sampling height is measured using a temperature probe (VMA324, Velleman; blue rectangle in Figure 2b). Both variables are logged onto an SD card via microcontroller (UNO, Arduino) housed inside a weatherproof container (Figure 2a, yellow case at lower left).

The Profiling module, with articulating arm. (a) Profiling module during field deployment. Inlet "head" in upper right of photo, with ultrasonic distance sensors encased in red plastic housing. Temperature sensor (not visible) located on opposite side of "head". Black winch in bottom left of photo controls inlet height via pulley system. Also visible in bottom left is the yellow case containing power supply and datalogger for temperature and distance sensors. Black tubing leading off to left connects to ISE-CUBE inlet. (b) Dimensional diagram for articulating arm.

While the descriptions of these two expansion modules are included here for completeness, only first-order assessments will ultimately be provided, as in-depth evaluation of the ISE-CUBE system is primarily focused on the performance of the analyzer in the Analyzer module (Sect. 4).

### 2.6 Field calibration expansion module (proposed)

Isotopic measurements obtained in the field require proper calibration before they can be interpreted. The calibration procedure involves providing the analyzer with a steady stream of vapor of known isotopic composition. These periods are subsequently used to calibrate the raw measurements on the international VSMOW2-SLAP2 (Vienna Standard Mean Ocean Water 2 - Standard Light Antarctic Precipitation 2) scale. It was our original intent to integrate a calibration module in the ISE-CUBE system, allowing for in-field daily calibrations. However, our field calibration system was not ready in time for our measurement campaign. Therefore, we calibrated the analyzer in a laboratory setting near to the deployment site immediately before and after deployment at each measurement site (see Sect. 3.3). Nevertheless, such a calibration module has the potential to be included in subsequent iterations of the ISE-CUBE system (see Sect. 6).

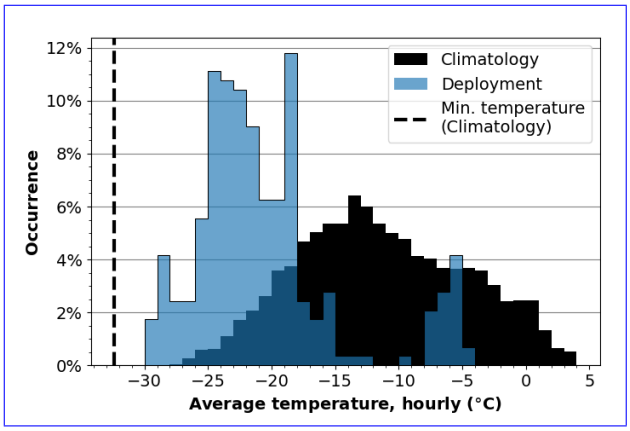


**Figure 4.** ~~Climatologies of temperature and wind in Ny-Ålesund. (a)~~ Histogram of hourly average temperatures in Ny-Ålesund for 2000–2019, 21 Feb to 14 Mar "Climatology" (black~~rectangles~~), alongside same from during the ISLAS2020 field campaign "Deployment" (~~purple bars~~blue). Black dashed line denotes minimum hourly temperature from the 2000–2019 period. ~~(b) Same as (a), but for hourly maximum wind speeds, with brown bars denoting "Deployment" conditions. Lines indicate maximum hourly wind gusts over climatology (black dashed) and deployment (brown dotted) periods. From~~ Data from *Norsk Klimaservicesenter, Ny-Ålesund (SN99910)*.

## 3 Performance test data sets

### 3.1 Campaign site and weather conditions

The performance of the ICE-CUBE system was evaluated based on a field campaign data set obtained in challenging Arctic measurement conditions at the scientific settlement of Ny-Ålesund, Svalbard (Figure B1), during the ISLAS2020 campaign. The principal aim of the ISLAS2020 field experiment was to obtain detailed in-situ measurements of isotope fractionation in a ~~cold, dry Arctic environment~~Arctic environment, characterized by open fjord water and snow surface. Ny-Ålesund, with the adjacent strong air-sea interaction in the Fram Strait, is a well-suited location to make such observations. In particular during winter and spring, this region is frequently subject to periods of strong marine cold-air outbreaks, associated with intense evaporation (Papritz and Spengler, 2017).

In Ny-Ålesund, we deployed at two measurement sites, the first being approximately 300 m south of Ny-Ålesund, on the tundra (78.921 17 °N,11.913 61 °E). This site was also referred to as the "Snow" location and was used from 25–28 Feb 2020. The second site was located on a concrete pier at the northernmost edge of the settlement (referred to as "Fjord"; 78.928 73 °N,11.935 52 °E), and was used from 7–14 March 2020. The Profiling module utilized the tripod frame while at the Snow site, while it used the tipping frame at the Fjord site, to reach further down towards the surface of the water.

General 2 m air temperature and 10 m wind speed and gust information for the Ny-Ålesund weather station (SN99910) were retrieved from the Norsk Klimaservicesenter (https://seklima.met.no/observations). From this station dataset, 20 year climatological conditions were established by considering the hourly dataset of the period between 21 Feb and 14 Mar, between 2000 to 2019. The time period from 21 Feb to 14 Mar in Ny-Ålesund has a climatological median air temperature for 2000–

2019 of −12 °C, with 50 % of hourly average temperatures being between −16 °C and −6 °C (Figure 4~~a, blackrectangles~~, black). In comparison, the majority of the ISLAS2020 campaign was spent in temperatures spanning −26 to −18 °C, with a median value of −20 °C (Figure 4~~a, purple bars~~, blue). The coldest temperatures experienced during the campaign (−30 °C) were comparable to the minimum temperature in the 2000–2019 climatology, −32.5 °C (Figure 4~~a~~, black dashed line). Overall, Feb and Mar 2020 were extreme conditions (Dahlke et al., 2022) to both test and measure with the system.

~~Climatological wind speed frequency peaks in the 2 to 3 $\mathrm{m\,s^{-1}}$ range (Figure 4b, black rectangles). Hourly maximum wind speeds during the field deployment (Figure 4b, brown bars) peak in the same range, though winds had a secondary peak in the 8 to 10 $\mathrm{m\,s^{-1}}$ range, twice the climatological frequency. With this distribution, we can classify winds during our observational period as mostly typical for the settlement. However, maximum wind gusts were still exceeding 20 $\mathrm{m\,s^{-1}}$ at times during the campaign (Figure 4b, brown dotted line). Overall, the deployment conditions presented a useful test case for the system. In addition to cold temperatures, the combination of high winds, low temperatures, and precipitation provide a reliable situation to evaluate if the systemwas still able to acquire stable and reliable measurement data.~~

### 3.2 Data processing

The ISE-CUBEs ~~produces three~~ produce two main data streams, pertaining to the Analyzer, ~~Cold Trap,~~ and Profiling modules~~.~~ , with each module internally recording its own respective stream. The Cold Trap expansion module does a similar task for its own data stream. An overview of the information contained in these ~~datasets are listed~~ data streams is given in Table 1. The isotopic ~~dataset~~ data stream generated by the analyzer in the Analyzer module is the primary dataset~~. The analyzer has been configured to measure at 4 Hz frequency, with the~~ , and also has the highest sampling frequency of 4 Hz. The primary environmental parameters observed ~~being~~ by the analyzer are humidity (volumetric mixing ratio), $\delta^{18}$O, and $\delta$D, alongside a multitude of analyzer diagnostic metrics~~.~~ , including temperatures and pressures internal components. ~~The dataset from the Analyzer module is generated and stored by the internal computer of the CRDS analyzer.~~ Before further use, the isotope data set was calibrated and corrected as described in Sec. 3.3 below.

Both the ~~Cold Trap and Profiling expansion~~ Profiling and Cold Trap modules measure at 1 Hz via Arduino microprocessors, and record parameters to SD cards. The ~~Cold Trap~~ Profiling module records the temperature at the inlet head, in addition to height distances measured by the ultrasonic sensors. Laboratory calibration of the temperature probe showed a systematic offset of 0.67 K, which is accounted for during post-processing. The Cold Trap expansion module monitors and records the flow through the collection vial, alongside remaining flow through the "bypass" line, as well as the temperature inside the module container. The same module also flags whether the cryogenic finger is within 5 K of the target temperature (−80 °C).

~~The Profiling module records the temperature at the inlet head, in addition to height distances measured by the ultrasonic sensors. Laboratory calibration of the temperature probe showed a systematic offset of 0.67 K, which is accounted for during post-processing.~~ Throughout the campaign, all module timestamps were compared to universal coordinated time, with offsets accounted for and datasets synchronised during processing.

~~A python script package (IsoFuse) then averaged each of the three data streams along a common time vector, and joined them into a netCDF file. While the technical analysis that will follow uses 1 s averaging with raw isotopic measurements,~~

**Table 1.** Parameters logged by the ISE-CUBE system. '*' indicates parameters classified as metadata, providing information on the quality of the data collected. '**' While flow rates and metadata of Cold Trap module are recorded as 1 Hz, sample collection times varied.

| heightModule | Parameter | Unit | Frequency |
|---|---|---|---|
| Analyzer | Isotopes ($\delta^{18}$O, $\delta$D) ~~,~~ | ‰ | 4 Hz |
| ~~Humidity,~~ | Humidity | $ppm_v$ | 4 Hz |
| ~~analyzer~~ | Analyzer diagnostics* | | 4 Hz |
| | (temperatures, ~~presures, etc.)~~ | °C | 4 Hz |
| | pressures, | Torr | 4 Hz |
| | spectrographic fits) | - | 4 Hz |
| Profiling | Inlet height | cm | 1 Hz |
| | Inlet temperature | °C | 1 Hz |
| Cold Trap | ~~Flows,~~ Flow rates | L/min | 1 Hz |
| | Module temperature* ~~,~~ | °C | 1 Hz |
| | Cryocooler temperature range* | [FLAG] ~~Profiling~~ | ~~Inlet height,~~ 1 Hz |
| ~~Inlet temperature~~ height | | | |

~~our~~ The analysis of module performance that will follow in Sect. 4 makes use of datasets averaged across multiple time intervals. The technical analysis of Analyzer module performance in Sect. 4.1 and 4.2 uses a 1 s averaged dataset, as does the assessment of the Profiling module sensors in Sect. 4.3. However, subsequent evaluation of the Profiling module in regards to sample transmission uses the native 4 Hz resolution. Based on our system characterizations evaluated below, our final calibrated isotopic profiling dataset is averaged over 30 s ~~periods (see~~ (Sect. ~~5).~~ 4.4 and 4.5).

### 3.3 Isotope calibration and data processing

~~Calibrations~~ Requisite calibrations of the analyzer were performed immediately preceding and following deployment at each measurement site, at the Marine Laboratory in Ny-Ålesund. ~~Two secondary standards , calibrated~~ We employed two secondary standards for analyzer calibration on the VSMOW2-SLAP2 scale~~at FARLAB, University of Bergen, Norway, were employed for calibration, namely~~ . The use of the VSMOW2-SLAP2 scale allows for the relative ratios of heavy to light isotopes ($R_{sample}$) measured in CRDS analyzers to be compared to an international standard ($R_{standard}$), as described in Eq. 1 (Craig, 1961).

$$\delta^* = \left( \frac{R^*_{sample}}{R^*_{standard}} - 1 \right) \cdot 1000 \qquad (‰) \tag{1}$$

The value of the resulting $\delta^*$, with $^*$ representing one of the heavy SWIs, is expressed in permil (per thousand, ‰). The two secondary standards used were, DI ($\delta^{18}$O~~: −7.68 ‰ =~~ $-7.68 \pm 0.07$ ‰ and $\delta$D~~: −49.71 ‰=~~ $-49.7 \pm 0.4$ ‰) and GSM1 ($\delta^{18}$O~~: −32.90 ‰ =~~ $-32.90 \pm 0.05$ ‰ and $\delta$D~~: −261.58 ‰). Standards =~~ $-261.6 \pm 0.3$ ‰). Liquid standards were delivered with the Standard Delivery Module (SDM) device (A0101, Picarro Inc.), utilizing a Drierite filled moisture trap as a source

of dry air. Only sufficiently stable calibration signals lasting longer than 10 minutes are considered for use in calibrating the dataset. As ~~mixing ratios~~ the specific humidity at the deployment site can be well below ~~6000 ppmv~~ 3.5 g/kg for the time of year, a correction of the isotope composition was applied during post-processing, according to the quantified mixing ratio – isotope ratio dependency by Weng et al. (2020), specific to the analyzer used in the field. Several calibrations made during the ISLAS2020 field deployment were between mixing ratios of ~~6000 ppmv and 850 ppmv~~3.5 g/kg and 0.5 g/kg, and confirm overall agreement with the mixing ratio – isotope ratio dependency determined in the laboratory.

~~Across 17~~ Calibrations performed in the Marine Laboratory were considered valid only if they passed automatic quality control thresholds, such as humidity variation below 0.3 g/kg (500 ppmv). Across 17 valid calibrations, DI measurements had a standard deviation of 0.15 ‰ for $\delta^{18}$O, and 0.48 ‰ for $\delta$D. ~~These are~~ For both isotope species, this standard deviation is similar (or smaller) ~~values for~~ than the standard deviation typical ~~of the individual calibrations~~during any individual calibration. Total measurement drift across the campaign duration for DI was found to be smaller than these standard deviations. The GSM1 standard experienced technical issues with the SDM during multiple calibrations. ~~Only 17 of the 28 calibrations passed automatic quality control thresholds, such as humidity variation below 500 ppmv.~~ The standard deviation across the 17 valid calibrations for this standard was 0.18 ‰ ($\delta^{18}$O) and 0.47 ‰ ($\delta$D), again of a similar magnitude to the variabilities seen in individual calibrations. ~~And as was also the case~~ As for DI, the total measurement drift across the campaign duration for GSM1 was found to be similar to or smaller than these standard deviations. Overall, these drift values are compatible with the behavior exhibited by the same analyzer during previous use in the lab and field (Weng et al., 2020; Chazette et al., 2021) and exceed the manufacturers typical performance specifications (Picarro Inc., 2021).

### 3.4 ~~Laboratory reference data~~Analyzer performance benchmark periods

~~The CRDS analyzercontained in the Analyzer module is designed for use in~~ We introduce two reference periods for comparison to our analyzer's behavior in the field. The first represents the optimal operating environment for the analyzer, a well-controlled laboratory ~~conditions. Therefore, we define a reference time period~~ setting, where the instrument routinely sampled standard vapor. This first period runs from June–July 2020 when the same analyzer was used at FARLAB, University of Bergen, Norway. ~~We use the two month period of June–July 2020 as a reference benchmark with regard to instrument and cavity temperature and pressure variations, which could influence the spectroscopy of the analyzer.~~ During this time, the analyzer was ~~in use for routine measurement operations~~ operating with ambient room temperatures of approximately 20 °C. ~~This routine measurement~~ Its operation included sampling mixing ratios down to ~~250 ppmv~~0.155 g/kg, comparable to ~~humidities~~ humidity minimums encountered in the field. The second period more closely resembles a typical deployment, with the instrument sampling exterior air through an inlet tube while installed inside a building with a controlled environment, but less stringently regulated than a university research laboratory. During this short-term deployment, the same analyzer was installed at the Zeppelin mountain observatory (475 masl), 2 km SSW of Ny-Ålesund. The installation spanned from 29 Feb 2020 to 2 Mar 2020, with the analyzer measuring outside the ISE-CUBE module. Both reference periods sampled at 1 Hz, and at a lower flow rate than we used in the field. Across the three environments, we compare the overall analyzer temperature, the cavity temperature and

pressure, and the temperature of the "warm box", an enclosure housing essential analyzer electronics critical for spectroscopic fitting.

### 3.5 Additional datasets

Since 2010 the Alfred Wegner Institute (AWI) has operated ~~an~~ the Ny-Ålesund eddy-covariance (EC) ~~station (Ny-Ålesund eddy-covariance site )~~ site (Jocher et al., 2012; Schulz, 2017), about 300 m south of the settlement and approximately 20 m away from the ISE-CUBE system during the initial deployment phase at Snow. This EC station measures, amongst others, air temperature ~~and winds at four heights: 0.5 m, 1.0 m, 1.5 m, and 2.5 m, with half-minutely resolution available~~at 1.0 m , averaged over 30 s. Temperatures are measured at ~~all levels by~~ by a Thies Clima compact temperature ~~sensors~~ sensor (2.1280.00.160, Adolf Thies GmbH & Co. KG, Germany), inside ~~ventilated shields~~ a ventilated shield (1.1025.55.100, Adolf Thies GmbH & Co. KG~~). Wind data are from Young propeller-style wind monitors (5106-5 (5103-5 @ 2.5 m), R. M. Young Company). Temperature and winds at 0.5 m were taken to be representative of ambient conditions while the ISE-CUBE system was deployed nearby, as detailed in Sect. 4.1. Additionally, temperature at 1.0 m~~ , Germany). This temperature was used for field validation of the temperature probe fixed to the head of the Profiling module, as described in ~~Sect. 4.3~~Appendix E.

~~A temporary EC station was also installed approximately 13 m away from the ISE-CUBE stack during the final phase of the campaign at the Fjord location. This setup included a Campbell Scientific CSAT3 sonic anemometer installed at 1.95 m above ground, providing 20 Hz measurement of wind and temperature. Minutely averages were derived from this high-resolution series, with less than 50 % low-quality data (as determined by internal CSAT3 diagnostics) over the minute. These measured conditions were taken to be representative of the ambient environment while the ISE-CUBE system was deployed at Fjord (Sect. 4.1).~~

## 4 Results

~~Now we~~ We now detail how the field conditions influenced analyzer performance and thus data quality, using the laboratory ~~performance as a benchmark.~~and observatory periods as performance benchmarks (Sect. 3.4). Thereby, we focus first on temperature and pressure conditions of the analyzer, before evaluating the impact of field conditions on the water isotope measurements. Then we detail the performance of the profiling module, including the onboard sensors, and also the modules capability to deliver sample to the analyzer for the purpose of resolving vertical profiles. Finally, the performance of the cold trap ~~and the profiling modules are~~ expansion module is briefly presented.

### 4.1 CRDS analyzer response to ambient conditions

Using our laboratory ~~benchmark, we will~~ and observatory benchmarks, we now detail how the field conditions influenced analyzer performance and thus data quality. We first ~~compare the overall temperature of the analyzer using the~~ use the Data Aquistion System (DAS) temperature (~~$T_{DAS}$~~) $T_{DAS}$) measured inside the analyzer housing as a proxy of the overall temperature and condition of the analyzer (Picarro Inc., 2013). Then, we ~~investigate~~ characterize the measurement cavity through its temper-

ature ($T_C$ $T_C$) and pressure ($p_C$ $p_C$). Finally, we study the essential analyzer electronics (Wavelength Monitor (WLM)) , namely the WLM, via the warm box temperature ($T_{WB}$ $T_{WB}$).

### 4.1.1 Overall analyzer temperature

The $T_{DAS}$ $T_{DAS}$ serves as a first-order proxy for the overall measurement environment of the analyzer. As the $T_{DAS}$ $T_{DAS}$ results from a balance between radiant, excess heat from other components (especially from the measurement cavity) and constant ventilation with ambient air, its value can span a wide range. In the laboratory, $T_{DAS}$ $T_{DAS}$ values are typically within a narrow distribution, with 94.5 % of $T_{DAS}$ 94.3 % of $T_{DAS}$ falling within the 45 to 50 °C bin 45 to 50 °C (Figure 5a, hatched bars). black). This narrow distribution is similar for the observatory (91.7 % within 47.5 to 52.5 °C). In contrast, the most frequent $T_{DAS}$ $T_{DAS}$ from the field is contained within the 30 to 35 °C bin (25.9 %) , and the overall distribution is markedly broader within the 30 to 32.5 °C range (17.3 %) (Figure 5a, green blue bars). The median $T_{DAS}$ is 11.9 °C lower in field, while Interquartile Range (IQR) is 4.5 times broader Across all percentiles (Table 2). , the $T_{DAS}$ in the field is lower and more broadly distributed. Thus, the overall temperature of the analyzer was colder and more variable in the field as compared to the lab. We now investigate the possible origin of these differences in $T_{DAS}$ However, the $T_{DAS}$ stayed within its necessary range for operation, with the analyzer remaining functional for the entirety of the two deployments. Therefore, any further impacts from this increased variability require exploration. We now continue our investigation with the conditions in the measurement cavity, the most critical element of the analyzer.

Since the $T_{DAS}$ partly results from ambient air ventilated into the analyzer, we now investigate how ambient conditions relate to $T_{DAS}$. Analyzer $T_{DAS}$ medians were between 28 to 46 °C, whereas ambient temperatures varied between −29 to −5 °C during the 12 different deployment days at the Snow and Fjord site (Figure **??**). Considering both measurement sites, the median daily $T_{DAS}$ (solid green line) exhibits a weak correlation (0.36) with daily mean temperature (Figure **??**a, purple line). As there should be some degree of connectivity between analyzer temperature and the temperature of environmental air being ventilated into the module, this relation fits with expectation. However, this relationship is decidedly more pronounced during the Fjord deployment (correlation of 0.95) than during the Snow (-0.44). This difference potentially arises from the fact that measurement operations at the Fjord site occasionally involved sliding the ISE-CUBE stack, during which time the incoming ventilation tubing for the Analyzer module would often come disconnected. This incoming tubing was connected to the exhaust of the Pump module, in an effort to pre-condition (i.e. slightly warm) the ventilating air. Upon disconnection, the Analyzer module would be directly exposed to cold ambient temperatures, resulting in lower analyzer temperatures. This highlights the potential value of such a pre-conditioning of the ventilation air for stable analyzer temperatures.

Analyzer response to ambient conditions from the two measurements sites of the ISLAS2020 field campaign (Feb: Snow, Mar: Fjord). a) Ambient daily temperatures and daily median $T_{DAS}$, as well as b) daily wind conditions alongside $T_{DAS}$ IQR. Median $T_{DAS}$ (green line) show a weak correlation (0.36) with mean ambient temperature at the deployment site (purple line), while interquartile range (IQR) of $T_{DAS}$ (green dashed line) exhibits a stronger anti-correlation (-0.66) with mean daily wind speed (brown line). Wind and ambient temperature measurements on 14 Mar affected by sea spray/icing, therefore daily values shown are taken to be representative, but actual daily values may differ.

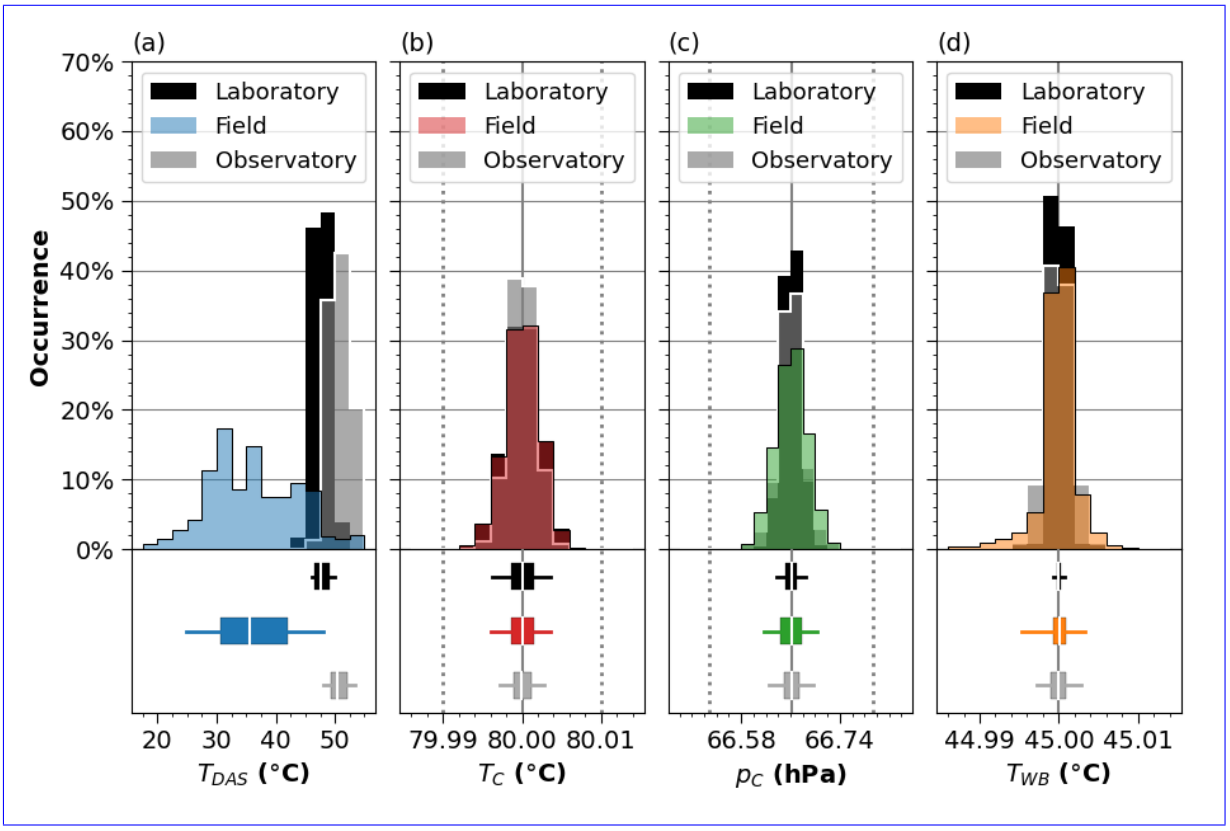


**Figure 5.** Relative occurrence of (a) DAS temperatures, ~~$T_{DAS}$~~ $T_{DAS}$ (~~5 °C~~ 2.5 °C bins), (b) Cavity temperatures, ~~$T_C$~~ $T_C$ (0.002 °C bins), (c) Cavity pressures, ~~$p_C$~~ $p_C$ (0.02 hPa bins), and (d) Warm Box temperatures, ~~$T_{WB}$~~ $T_{WB}$ (0.002 °C bins) during CRDS operation, for field deployment periods (colored~~bars~~) as compared to reference periods, laboratory ~~benchmark (hatched bars~~black) and observatory (gray). Lower panels show total distributions for the three periods in boxplot form, with the median (white line), IQR (box limits), and 95$^{th}$ and 5$^{th}$ percentiles (whiskers). Solid vertical lines for b), c), and d) indicate parameter target value. Dotted lines for b) and c) indicate instrument control precision as per manufacturer. Note that "Field" and "Laboratory" overlap closely in b).

~~A second environmental factor that may have a connection to analyzer temperature and temperature stability is the wind speed. Wind speeds were relatively low at the Snow site (2 to 6 $\mathrm{m\,s^{-1}}$), but ranged up to 13 $\mathrm{m\,s^{-1}}$ during the Fjord deployment (Figure ??b). Daily DAS IQR (Figure ??b, green dashed line) and mean daily wind speed (brown line) shows the largest IQR values occur during days with low wind speeds. When considering all days, the two curves have a moderate anti-correlation ($-0.66$), indicating higher $T_{DAS}$ variability on days with low wind speeds. It is likely that this is an indirect relationship, influenced more by the impact that wind speed had on the extent of operations that we did on any particular day. On days with higher winds, we kept operations to a minimum, simply performing routine checks and switching collection vials in the Cold Trap, both of which involved removing the protective canvas cover for a only short time (see Figure C1). However, during less windy days (Figure C2), our operations were more extensive. We would conduct multiple profiles with the cover removed~~

**Table 2.** Analyzer ~~temperature~~ statistics ~~in °C. 25th, 50th~~ for the overall analyzer temperature (~~median~~$T_{DAS}$), the cavity temperature and ~~75th percentiles of DAS~~ pressure (~~$T_{DAS}$~~ $T_C$ and $p_C$), ~~Cavity ($T_C$),~~ and ~~Warm Box temperatures~~ the warm box temperature (~~$T_{WB}$~~ $T_{WB}$). Percentile intervals as indicated from field, laboratory, and ~~field~~observatory periods. ~~Interquartile range (IQR)~~ Corresponding 95th to 5th span provided for the same.

| | | Percentile | | | | | |
|---|---|---|---|---|---|---|---|
| | ~~25th~~ Location | ~~50th~~ 5th | ~~75th~~ 25th | ~~IQR~~ 50th | 75th | 95th | 95th-5th |
| height | Lab | 46.1 | 46.6 | ~~47.5~~ 47.6 | ~~49.0~~ 49 | ~~2.4~~49.9 | 3.8 |
| $T_{DAS}$ (°C) | Obs | 48.0 | 49.2 | 50.3 | 52.2 | 53.4 | 5.4 |
| | Field | 24.8 | 30.8 | 35.6 | 42.1 | ~~11.3~~48.0 | 23.2 |
| height | Lab | ~~79.9986~~ 79.996 | ~~80.0000~~ 79.999 | ~~80.0015~~ 80.000 | ~~0.0029~~80.001 | 80.004 | 0.008 |
| $T_C$ (°C) | Obs | 79.997 | 79.999 | 80.000 | 80.001 | 80.003 | 0.006 |
| | Field | ~~79.9986~~ 79.996 | ~~80.0001~~ 79.999 | ~~80.0015~~ 80.000 | ~~0.0029~~80.001 | 80.004 | 0.008 |
| height | Lab | ~~44.9997~~ 66.64 | ~~45.0000~~ 66.65 | ~~45.0002~~ 66.66 | ~~0.0005~~66.67 | 66.69 | 0.05 |
| $p_C$ (hPa) | Obs | 66.63 | 66.65 | 66.66 | 66.67 | 66.70 | 0.07 |
| | Field | ~~44.9993~~ 66.62 | ~~45.0001~~ 66.64 | ~~45.0009~~ 66.66 | ~~0.0016~~66.68 | 66.70 | 0.08 |
| height | Lab | 44.999 | 45.000 | 45.000 | 45.000 | 45.001 | 0.002 |
| $T_{WB}$ (°C) | Obs | 44.997 | 44.999 | 45.000 | 45.001 | 45.003 | 0.006 |
| | Field | 44.995 | 44.999 | 45.000 | 45.001 | 45.003 | 0.008 |

~~and the analyzer temperature variability would increase. This result points to the system's potential value as a more fixed measurement platform, one without daily disturbances. It also highlights the benefit of having a protective cover to serve as a windbreaker for the stack modules. Therefore, after considering this wind speed/operation relationship, the direct impact that the wind speed has on analyzer temperature is negligible in comparison.~~

~~In summary, the ambient conditions (especially temperature) did generally affect the internal analyzer temperature, and lead to more variable and overall colder $T_{DAS}$. However, the $T_{DAS}$ remained within its nominal range of operation, with the analyzer remaining functional for the entirety of the two deployments. We now continue our investigation with the conditions in the measurement cavity, the most critical element of the analyzer.~~

~~(a) CRDS analyzer cavity temperature as a function of DAS temperature. Cavity temperature target is $80.00 \pm 0.01$ °C. Daily median indicated with black tick inside solid colored bar, upper and lower extents indicate 75th and 25th percentiles, respectively. Whiskers denote 98th and 2nd percentiles. Background shading denotes IQR from laboratory benchmark. (b) Same as (a), but for the Warm Box temperature with a target of 45 °C.~~

### 4.1.2 Cavity temperature and pressure

The precision and accuracy of the temperature inside the measurement cavity of the analyzer is of the utmost importance for precise spectroscopic measurements. For this reason, the analyzer regulates the cavity temperature very precisely about

$80.00 \pm 0.01$ °C (Steig et al., 2014). Median $T_C$ for the entire fielddeployment was 80.0001 °C (Table 2), only 0.0001 °C higher than the target and our laboratorybenchmark value, and indistinguishable from the laboratory The median $T_C$ is identical across the field, laboratory, and observatory periods, 80.000 °C (Figure 5b ). Additionally, IQR from field and lab were identical to 0.1 mK (and Table 2). Across the aforementioned $T_{DAS}$ bins, 96 % of the variation about the 80 °C target was within 0.005 °C while in the lab. This is the same extent of variation that is present in the fielddata (whiskers of Figure **??**a, 98Between the 95$^{th}$ and 2$^{nd}$ percentiles). The median of 5$^{th}$ percentiles, $T_C$ distributions between field and laboratory are indistinguishable from one another. In the field, the cavity temperature from the field (black ticks) is below target at the extreme ends of DAS operating conditions ($-0.0005$ °C in the 15 to 20 °C range and $-0.0002$ °C in the 50 to 55 °C range). However, these bins together only constitute 4.4 % of the total observations, and are still within acceptable limits. Furthermore, IQR from the field (Figure **??**a, red boxes), including the two extreme bins, is of the same magnitude ($\pm 0.0015$ °C) as the IQR of the laboratory (shaded area)stays within this range for 99.99 % of the time, which exceeds the laboratory benchmark (99.97 %). Finally, there exists no correlation (0.000) between $T_C$ and $T_{DAS}$ while deployed in the field. Therefore, 95.6 % 99.99 % of field observations are made with cavity temperatures typical of the laboratory, with the remaining 4.4 % being only slightly atypical in the median, but still within specified limits., and are indistinguishable from the laboratory benchmark.

The pressure inside the analyzer cavity must be maintained at $66.66 \pm 0.10$ hPa (Steig et al., 2014). This range is maintained for 99.95 % of the field deployment (Figure 5c). Since the The ISE-CUBE system does very little to modify the native flow pattern of the analyzer, therefore we expect that the $p_C$ $p_C$ exhibits no dependence on the DAS temperature. Just as with $T_C$, there is no correlation (0.000) between $p_C$ and $T_{DAS}$ while deployed in the field. Overall, the specified range is maintained for 99.95 % of the field deployment, nor the fielddeployment in general. which differs from our laboratory benchmark (99.99 %). Indeed, on any of the 12 deploymentdays, the $p_C$ was within the 0.1 hPa specification 99 % of the time, with a maximum IQR of 0.048 hPa. Across the same DAS bins used in cavity temperature analysis, the maximum departure of $p_C$ median from the target is 0.0005 hPa. However, when the entire deployment as a whole is considered, the distribution about the target is broader in the field as compared to the lab both the laboratory and observatory reference periods have slightly narrower distributions (Figure 5c ). In fact, variability about the target (IQR: 0.035 hPa) is 75 % greater than what is typically found during the laboratory benchmark (IQR: 0.020 hPa).

and Table 2). So even though the cavity pressure remained within limits for the vast majority of the time, some aspect of the field deployment had an impact on cavity variability. After further investigation into other potential differences between the laboratory and field setups, it was we determined that this difference in cavity pressure stability variability stems from the enhanced sample flow configuration of the analyzer while being used in the field (Sect. 2.2), and is not inherent to a specific aspect of the ISE-CUBE system. The fast-response configuration on this instrument has been used in a previous field deployment (Chazette et al., 2021), and is within the scope of the standard operating procedures.

In summary, the accuracy and precision of cavity pressure and temperature remained within specified limitsnecessary limits, and were comparable to our two benchmark periods. In particular, the cavity temperatures were nearly indistinguishable between laboratory and field. We therefore expect reliable functioning of the measurement cavity of the analyzer to have been functioning reliably during the field deployment. As a final analyzer parameter, we now investigate the warm box temperature.

### 4.1.3 Warm Box temperature

The WLM is part of the analyzer's laser control loop and is continuously used to target the desired wavelengths, reducing instrument drift (Crosson, 2008; Gupta et al., 2009). It is contained within the Warm Box, which the analyzer regulates the interior temperature ~~of~~ to 45 °C. In our laboratory benchmark, ~~more than 50 %~~ 90 % of the variation about this target was within ~~0.0003 °C~~ 0.002 °C (Table 2). ~~Considering the entire field deployment, $T_{WB}$ distribution is broader~~ In comparison, the same range of $T_{WB}$ in the field~~as compared to the laboratory (Figure 5d), with an IQR approximately three times larger~~ , has four times the variability (Table 2). ~~Considering $T_{WB}$ across DAS bins, the size of the IQR in the field was up to 6 times larger than in the laboratory~~ The field distribution is more similar to our observatory benchmark period (Figure ~~??b, orange rectangles and shaded area). Additionally, the field medians of the two lowermost and the uppermost $T_{DAS}$~~ 5d and Table 2). Even when compared to this benchmark, $T_{WB}$ from the field has a tendency towards lower temperatures (Figure ~~??b, black ticks)are lower than even the 25$^{th}$ percentile of the laboratory period~~5d). This indicates that the temperature inside the Warm Box is coupled to the changing (usually cooling) analyzer temperature. Since the analyzer has a gas inlet at the back, leading to the WLM, ambient air temperature could also more directly impact the ~~$T_{WB}$~~ $T_{WB}$ than other components. As an example, sudden dips and spikes in ~~$T_{WB}$~~$T_{WB}$ correspond with the onset of drops and rises in ~~$T_{DAS}$~~$T_{DAS}$ (Figures C1 ~~&~~and C2). As this range of variations could potentially have an impact on measurement quality, we now assess WLM performance in more detail during lab and ~~field~~benchmark.

For the evaluation of the WLM performance, we use three spectroscopy metrics that quantify the difference between an expected model spectrum versus the fitted absorption spectrum that is actually measured by the analyzer (Johnson and Rella, 2017). The baseline shift (BS) describes the absolute value change of the spectral baseline, the slope shift (SS) indicates the change in the slope of the baseline (Johnson and Rella, 2017; Weng et al., 2020), and the residual (RS) represent the residual errors present in the fit spectrum, compared to the expected spectrum. The spectra have a first-order dependency on mixing ratio with resulting baseline differences (Aemisegger et al., 2012; Steen-Larsen et al., 2013, 2014b; Bonne et al., 2014; Weng et al., 2020). To account for this dependency on the isotopic concentrations derived from the spectra, data from both ~~laboratory and field~~ field and reference periods have been sorted into ~~300 ppmv~~ 0.075 g/kg bins, from ~~300 to 3900 ppmv.~~ 0.150 to 2.400 g/kg. For field measurements, only instances when the $T_{WB}$ is above the 95$^{th}$ or below the 5$^{th}$ percentiles are considered. In our laboratory benchmark, only periods using synthetic air (80 % $N_2$, 20 % $O_2$) as a carrier gas are considered. Specifically, these periods consist of seven multi-point humidity calibrations (Figure D1, d-j) with a lab standard being of a similar depletion ($\delta^{18}$O: $-40.02 \pm 0.07$ ‰ and $\delta$D: $-307.8 \pm 0.8$ ‰) as the field.

Figure 6 displays a comparison between the three metrics during ~~laboratory~~ reference periods against field operation. Ideal analyzer performance would produce a strong correlation in the three metrics between ~~laboratory and field~~ field and reference data, while also aligning closely to a 1-to-1 line. ~~The~~ All three metrics have correlations ~~of 0.994 (BS), 0.980 (SS), and 0.959 (RS~~above 0.990, for both laboratory and observatory (Table 3). Additionally, our two reference periods have comparable values, at similar specific humidity concentrations (Figure 6). The BS and SS also have linear regression line slopes near to 1~~(0.90 ± 0.06 and 1.04 ± 0.14, respectively, Figure 6a and b)~~. The RS error has the linear regression with the largest deviation

from 1, (~~0.75 ± 0.15~~1.35 ± 0.03 and 1.49 ± 0.11, for laboratory and observatory, respectively) with an intercept ~~of 0.05 ± 0.03~~ ~~(Figure 6c~~within 0.02 (Table 3). While analyzer performance to first order appears as desired, ~~the~~ this consistently larger RS error of the ~~lowest humidities~~ field indicates that the spectral fit in the field ~~deviated further compared to the lab. Thus, measurements at low humidity could be less accurate measurements in the field.~~

~~(a) Baseline Shift, (b) Slope Shift, and (c) Residuals of the expected model spectrum versus the fitted absorption spectrum from the analyzer's WLM. Light gray line represents 1-to-1 ratio. Data are divided into 300 ppmv bins, from 300 to 3900 ppmv (colorbar), with error bars denoting IQR for both lab and field measurements. Dotted lines indicate linear regressions through the data points, with gray shading showing the 95 % confidence interval.~~

~~Interestingly, the opposite is suggested at the higher humidities (>3300 ppmv), with a tendency for higher RS values in the lab (i. e. better spectroscopic fitting~~ was not as good as in the reference periods. The fits are also similar when all $T_{WB}$ values are considered and not only above the 95$^{th}$ or below the 5$^{th}$ percentiles. While this indicates that the measurements in the field ~~). Such a peculiar result can be reconciled by considering what other factors can influence the spectroscopy. Aside from the mixing ratio, the spectroscopy can also be affected by the exact composition of the air or carrier gas, including the presence of organic contaminants (Johnson and Rella, 2017). In our laboratory benchmark, both pure nitrogen (100 % $N_2$) and synthetic air (80 % $N_2$, 20 % $O_2$) were used as carrier gases, which can cause spectroscopic differences from our field deployment. Consequently, a precise match is unlikely. Therefore, unlike analyzer metrics such as temperatures and pressure, deviations of WLM metrics from the expected 1-to-1 relationship do not allow a final conclusion with regard to the effect of WLM temperature variation on field measurements~~ have the potential for larger uncertainty, obtaining an exact quantification of uncertainty from this difference is non-trivial and requires access to proprietary analyzer details. Therefore, we now proceed with an alternative method to quantify the quality of the water isotope measurements from the ISE-CUBE system.

**Table 3.** Correlations and linear regression values (slope and intercept) for WLM metrics (Baseline shift, BS; Slope shift, SS; and Residuals, RS) in field vs. ~~laboratory and observatory~~reference period.

| | | Field vs. | |
|---|---|---|---|
| | | Laboratory | Observatory |
| **BS** | Correlation | ~~0.994~~ 0.999 | 0.995 |
| | Slope | ~~0.90 ± 0.06~~ 0.99 ± 0.01 | ~~1.02 ± 0.03~~ 1.07 ± 0.06 |
| | Intercept | ~~−0.37 ± 0.59~~ −0.42 ± 0.07 | ~~0.07 ± 0.21~~ −0.03 ± 0.18 |
| **SS** | Correlation | ~~0.980~~ 0.998 | ~~0.999~~ 0.995 |
| | Slope | ~~1.04 ± 0.14~~ 0.88 ± 0.02 | ~~0.84 ± 0.02~~ 0.86 ± 0.05 |
| | Intercept | ~~0.02 ± 0.65~~ 0.08 ± 0.08 | ~~0.24 ± 0.13~~ 0.16 ± 0.16 |
| **RS** | Correlation | ~~0.959~~ 0.991 | ~~0.990~~ 0.991 |
| | Slope | ~~0.75 ± 0.15~~ 1.34 ± 0.05 | ~~0.96 ± 0.09~~ 1.49 ± 0.11 |
| | Intercept | ~~0.05 ± 0.03~~ 0.00 ± 0.01 | ~~0.03 ± 0.02~~ −0.02 ± 0.01 |

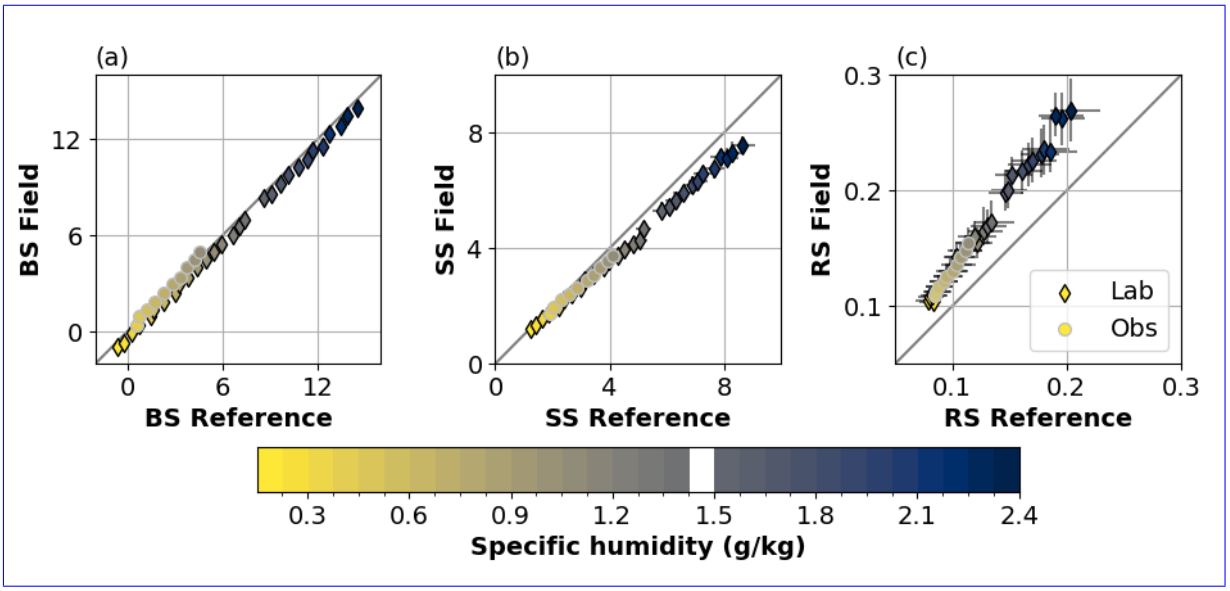


**Figure 6.** ~~Kernel density estimations for~~ (a) ~~Warm Box temperature~~Baseline Shift, (b) ~~DAS temperature~~Slope Shift, and (c) ~~Cavity temperature. Colored, thick, and dashed lines represent values~~ Residuals of the expected model spectrum versus the fitted absorption spectrum from ~~field~~the analyzer's WLM, ~~observatory, and laboratory, respectively~~for field periods where the warm box temperature is above the 95$^{th}$ or below the 5$^{th}$ percentiles. ~~Curves have been smoothed to improve visualization~~Light gray line represents 1-to-1 ratio. ~~Note that "Field" curves overlap closely with with "Obs"~~ Data are divided into 0.075 g/kg bins, from 0.15 to 2.4 g/kg (~~Observatory~~colorbar)~~and "Lab" (Laboratory) curves in (a) and (c)~~, ~~respectively~~with error bars denoting IQR for both field and reference measurements.

~~As the difference between our laboratory benchmark and field deployments prevent further conclusions, we now use measurements with our analyzer during a short-term deployment at the Zeppelin mountain observatory (475 masl, 2 km SSW of Ny-Ålesund. This intermediate operation in a semi-regulated environment provides us with a secondary benchmark in the WLM performance evaluation. The analyzer was installed at Zeppelin observatory from 29 Feb 2020 to 3 Mar 2020, without the ISE-CUBE system and measuring ambient air. When similarly comparing the WLM metrics from the field deployment with those of the observatory, the results and uncertainties are closer to expectations (Table 3 and Figure **??**). Correlations of all spectroscopic metrics are also improved. Additionally, the distribution of $T_{WB}$ during observatory (Figure **??**a, thick gray) and field (orange) deployments are similar. However, $T_{DAS}$ in the observatory (Figure **??**b) are much more similar to laboratory conditions (dashed), than to field (green). This indicates that $T_{WB}$ variability is not only controlled by ambient analyzer temperatures. Finally, $T_C$ distributions are similar across all three locations (Figure **??**c), demonstrating that the cavity was able to maintain temperature within an acceptable range, regardless of deployment location.~~

~~Then to summarize, the measurement cavity remained mostly unaffected, and the warm box maintained a temperature at the same quality as of a field laboratory. We can now therefore proceed to quantify the quality of the water isotope measurements from the ISE-CUBE system.~~

### 4.2 Measurement quality of water vapor isotopes

Based on the assessment of analyzer parameters presented above, measurement conditions within the ISE-CUBE system and in the laboratory differ mostly with respect to the variability of ~~$T_{WB}$ and $T_{DAS}$~~ $T_{WB}$ and $T_{DAS}$. To identify a potential impact of this temperature variability on the vapor isotope measurements, we now compare the variability of the isotopic signal between ~~laboratory and~~ our reference periods and the field. Since mixing ratio (and thus the amount of molecules in the measurement cavity) is a key factor in the precision of the CRDS measurements, we divide the measurement data into ~~the same~~ 15 bins from 0.150 to 2.400 g/kg, 0.150 g/kg wide; similar to the bins as we used before ~~(Section 4.1.3). For each bin and for each day in the field, we identify the 5 minute period~~ in Sect. 4.1.3, though twice as wide.

For our field period, we first partition our measured humidities by site; in this way, we ensure that measurement conditions at each site are represented. Then, we identify the distribution of measured humidities at each site according to our bins, and normalize it to 100 for the Snow site and 200 for the Fjord site. Then, occurrence in each bin is rounded up to the nearest whole number, such that the smallest bin contains at least two points. Finally, for each site and bin, we identify a corresponding number of 5 minute windows with the most stable mixing ~~ratio~~ ratios (i.e. lowest standard deviation ~~); the mixing ratio must stay within the bin range for at least 50 % of the time during this 5 minute window (i. e. necessary for periods close to bin edges)~~of humidity), as categorized by the mean across the 5 minutes. The maximum standard deviation across all 5 minute windows in the field was 0.030 g/kg, with the median being 0.002 g/kg. A similar procedure was done for the observatory reference period, though standard deviations were lower than in the field. Within the laboratory benchmark, ~~rather than daily periods,~~ we focus on ~~eight~~ ten distinct usage events conducted for instrument characterization purposes (Figure D1). During these ~~usage~~ events, the analyzer was subjected to step-wise mixing ratio sequences between ~~400 and 3900 ppmv (Figure~~0.20 and 2.25 g/kg (Figure D1). The steps usually lasted 5 to 10 minutes, and the sequences did not necessary follow a consistent step magnitude. Similarly as to the field and observatory, the most stable 5 minute window were identified, using a cut-off threshold of 0.006 g/kg. These sequences used a standard of a similar depletion ($\delta^{18}$O: ~~−40.02 ‰,~~ $-40.02 \pm 0.07$ ‰ and $\delta$D: ~~−307.79 ‰~~ $-307.8 \pm 0.8$ ‰) as our field measurements. ~~By identifying periods this way, we prevent over-sampling of low mixing ratios or specific fielddays, while still generating a sample population representative of mixing ratios encountered in the field. The~~ For laboratory, observatory, and field, the 1-$\sigma$ 5 minute standard deviation over each of these ~~periods~~ windows was then calculated for both $\delta^{18}$O and $\delta$D.

For ~~the laboratory and field~~ all three periods, and for both $\delta^{18}$O and $\delta$D, the measurement precision decreases with decreasing mixing ratio (Figure 7a,c). ~~While standard deviations of the laboratory are approximately constant above 3000 ppmv, in~~ The same is true of the d-excess (Figure 7e). In the lowermost bin of ~~300 to 600 ppmv, 5-min~~ 0.150 to 0.300 g/kg, 5 minute standard deviations in the field reach up to ~~0.9 ‰~~ 1.0 ‰ for $\delta^{18}$O (Figure 7a), and ~~7 ‰~~ 8 ‰ for $\delta$D and the d-excess (Figure 7c~~). Field~~ ,e), whereas the same in the laboratory reference are around 0.7 ‰ ($\delta^{18}$O) and 5 ‰ ($\delta$D and d-excess). Across all humidities, field bin means (~~blue~~ thick colored line) are consistently higher than laboratory and observatory bin means (~~black line)across all humidities. However, when considering the bin means, the difference between the laboratory and the field is never more than 0.08 ‰~~ Figure 7a,c,e; black and gray/white lines, respectively). This difference between field and reference

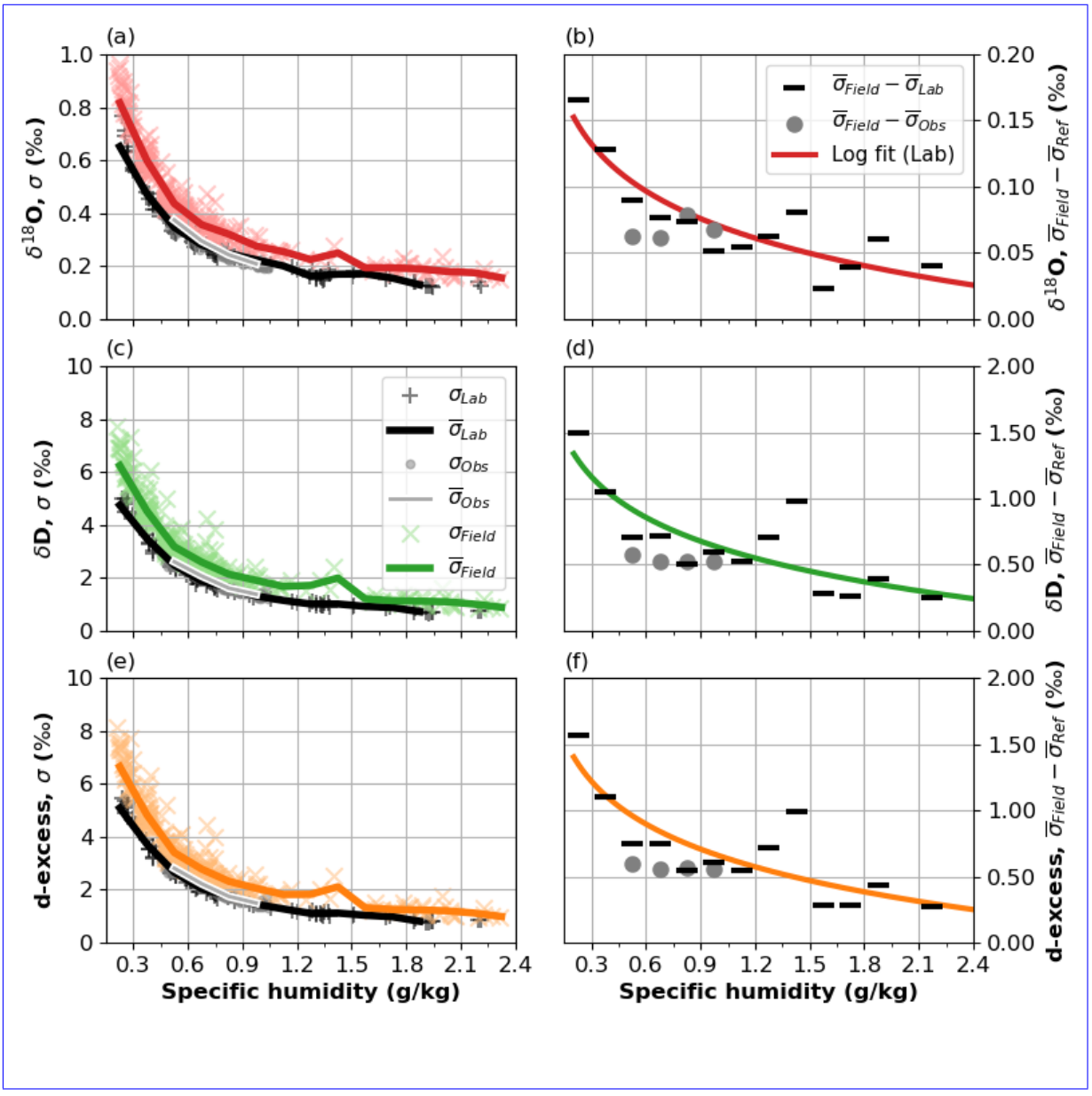


**Figure 7.** Standard deviations of $\delta^{18}$O~~and~~ , $\delta$D~~in laboratory~~ , and d-excess in field and reference periods, alongside differences between ~~the two,~~ periods. Measurements organized across ~~300 ppmv~~ 0.15 g/kg bins, from ~~300 to 3900 ppmv~~0.15 to 2.40 g/kg. (a) Standard deviations of $\delta^{18}$O over 5 min periods from field (~~blue~~ colored '~~+~~x')~~and~~ , laboratory (black '+', and observatory (gray '~~x~~o')); see text for details. Bin means depicted with ~~blue (field) and black (laboratory)~~ thick lines. (b) Difference between bins means from field and laboratory (black ticks) and field and observatory (gray circles) periods. ~~Dashed blue~~ Thick colored line ~~is~~ indicates the ~~median, while shading shows IQR~~logarithmic fit of field-lab differences. (c,d) Same as (a,b) but for $\delta$D. (e,f) Same as (a,b) but for d-excess.

periods (Figure 7b~~) and 1.0 ‰~~ ,d,f) increases at lower humidities, and is consistent between reference periods. A logarithmic fit (Figure 7~~d), ~~ b,d,f; thick colored lines) gives the maximum increase in measurement uncertainty (at the minimum humidity value from the field, 0.197 g/kg) as 0.15 ‰ for $\delta^{18}$O ~~and~~ , 1.35 ‰ for $\delta$D, ~~respectively. The overall median difference across all bins is 0.06 ‰ and 0.47 ‰ for~~ and 1.42 ‰ for d-excess. According to this fit, the median humidity value from the field (0.562 g/kg) would have associated increases of uncertainty in $\delta^{18}$O ~~and~~ , $\delta$D~~.~~ , and d-excess of 0.10 ‰, 0.89 ‰, and 0.93 ‰, respectively. Averaged across humidity bins, this variability increase in the field is approximately 30 % more than the variability in the laboratory benchmark, though the largest relative increase occurs at the higher humidities.

In summary, the ~~two field deployment locations exhibit consistently lower measurement precision of both isotope species. This lower precision~~ field deployment exhibits consistently higher variability for isotopic measurements, as compared to the optimal measurement conditions in a well-controlled research laboratory. This higher variability in the field is likely a consequence of the more variable ~~$T_{WB}$ and $T_{DAS}$, as well as~~ $T_{WB}$ and $T_{DAS}$, but could also be due to the more variable composition of the ambient air ~~. Nonetheless, differences to measurements in a laboratory environment are quite limited, and do~~ used to quantify stability. Additionally, we have not investigated the contribution that our increased flow configuration (Sect. 2.2) might have on this increase in variability. Therefore, we proceed under the premise that our obtained measurements have an increased uncertainty associated with the conditions and the deployment system, as described by the calculated logarithmic fits. Nonetheless, we will show that this decreased precision does not hinder useful measurements, in particular ~~if~~ since the measurement precision is quantified and can be applied to the observations.

### 4.3 Profiling module performance

Evaluation of the Profiling module is divided into sensor performance and sample transmission. Sensor performance details of the the ultrasonic distance sensor and the temperature probe at the tip of the inlet are found in Appendix E. We now assess the Profiling module's ability to transmit sample to the analyzer, including its capacity to resolve isotopic profiles.

The time it takes for the analyzer to react to a step change in humidity at the inlet head is predominantly governed by the length of the inlet tubing and the flow rate through it. With the heated tubing from inlet tip to the sample port of the analyzer having a diameter of 4.5 mm, and at a flow rate of about 9 L min$^{-1}$ in the Profiling module tubing, and 0.15 L min$^{-1}$ in the inlet assembly, the minimum response time would be approximately 6 s. We were unable to conduct any controlled single-step changes during the field deployment, as we lacked a suitable field device to produce a defined vapor isotope stream at sufficiently high flow rates. However, profiling with the articulating arm approximated multiple step changes, albeit without a controlled humidity source. We take the profiling period from the Fjord site on 9 Mar 2020, which included multiple abrupt humidity changes as we stepped through profiling levels, with some step changes reaching 0.3 g/kg (Figure 8a). Therefore, we followed the approach of Steen-Larsen et al. (2014b) and Wahl et al. (2021), and applied a fast Fourier transform analysis to the normalized time derivative of the specific humidity observed during this profiling period (Figure 8b). We then consider the median across 20 logarithmically spaced bins, between $5.55 \times 10^{-3}$ and 2 Hz, of the resulting power spectra as a signal to noise ratio (SNR) (Figure 8b, blue line), with the spectral minimum defining our baseline at approximately 0.4 Hz or 2.5 s. We see that the signal reaches 63 % of its full response after approximately 20 s, however, by 30 s the signal is 80 % of full response.

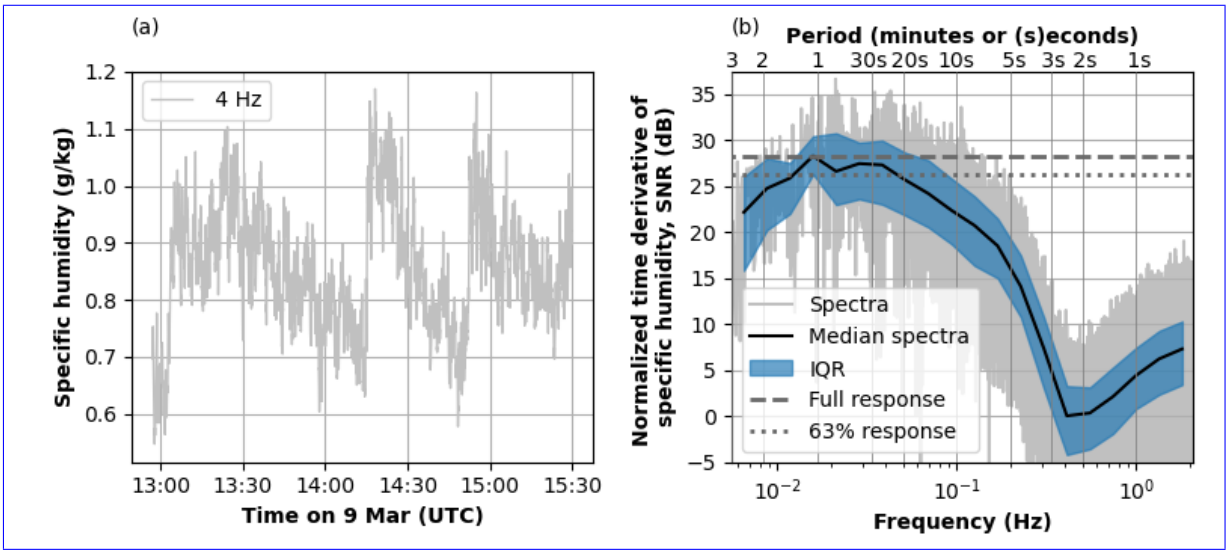


**Figure 8.** Inlet response determination for the profiling period on 9 Mar 2020, from 12:57 to 15:30 UTC. (a) The 4 Hz specific humidity signal as measured by the analyzer. (b) The fast Fourier transform of the normalized time derivative of the specific humidity (gray), expressed as a signal to noise ratio. Black line is the median of the resulting power spectra, across 20 logarithmically spaced bins between between $5.55 \times 10^{-3}$ and 2 Hz, while colored shading is the interquartile range (IQR) of the bin. The minimum of the median (at approximately 0.4 Hz or 2.5 s) serves as noise baseline, where as the maximum signifies the full response (dashed gray line). Dotted line indicates 63 % of the full response.

These statistics are also similar, though less strong, for the low humidities encountered at the Snow site (see Supplemental Material). Therefore, we conclude that the system is capable of producing a dataset with 30 s resolution, which can be used for analysis purposes.

Next, we consider the minimum duration required at a particular height to resolve the isotopic profile. We again take our profiling period on 9 Mar 2020, now examining the isotopic measurements (Figure 9a,c,e). We apply a fast Fourier transform on the 4 Hz isotopic signal to obtain a power spectrum across a range of frequencies/periodicities (Figure 9b,d,f). The spectra median (across 20 logarithmically spaced bins between $8.33 \times 10^{-4}$ and 2 Hz) (Figure 8b,d,f; thick black lines) indicate a baseline extending from 2 Hz until approximately 0.1 Hz (10 s). Frequencies higher (periodicities smaller) than this are considered to be indistinguishable from noise. The 25$^{\text{th}}$, and especially the 75$^{\text{th}}$ percentiles for these frequencies are also mostly constant (Figure 9b,d,f; colored shading). At periods larger than 20 s, the signal begins to emerge from the noise. The d-excess signal takes the longest to emerge, with the median SNR surpassing the 75$^{\text{th}}$ percentile of the noise level (Figure 9f; dotted line) at 1.5 minutes. This means that 50 % of the frequencies at this point have a higher SNR than 75 % of the noise. Periodicities smaller than this have less than twice as much power as the noise median, and cannot be resolved. After 2 minutes, the median signal reaches 5 dB, or approximately 3.16 times the median noise baseline; periodicities larger than this can begin to be resolved. At periodicities of 4 minutes, medians of all isotopic signals have an SNR larger or equal to 10 dB. At the less

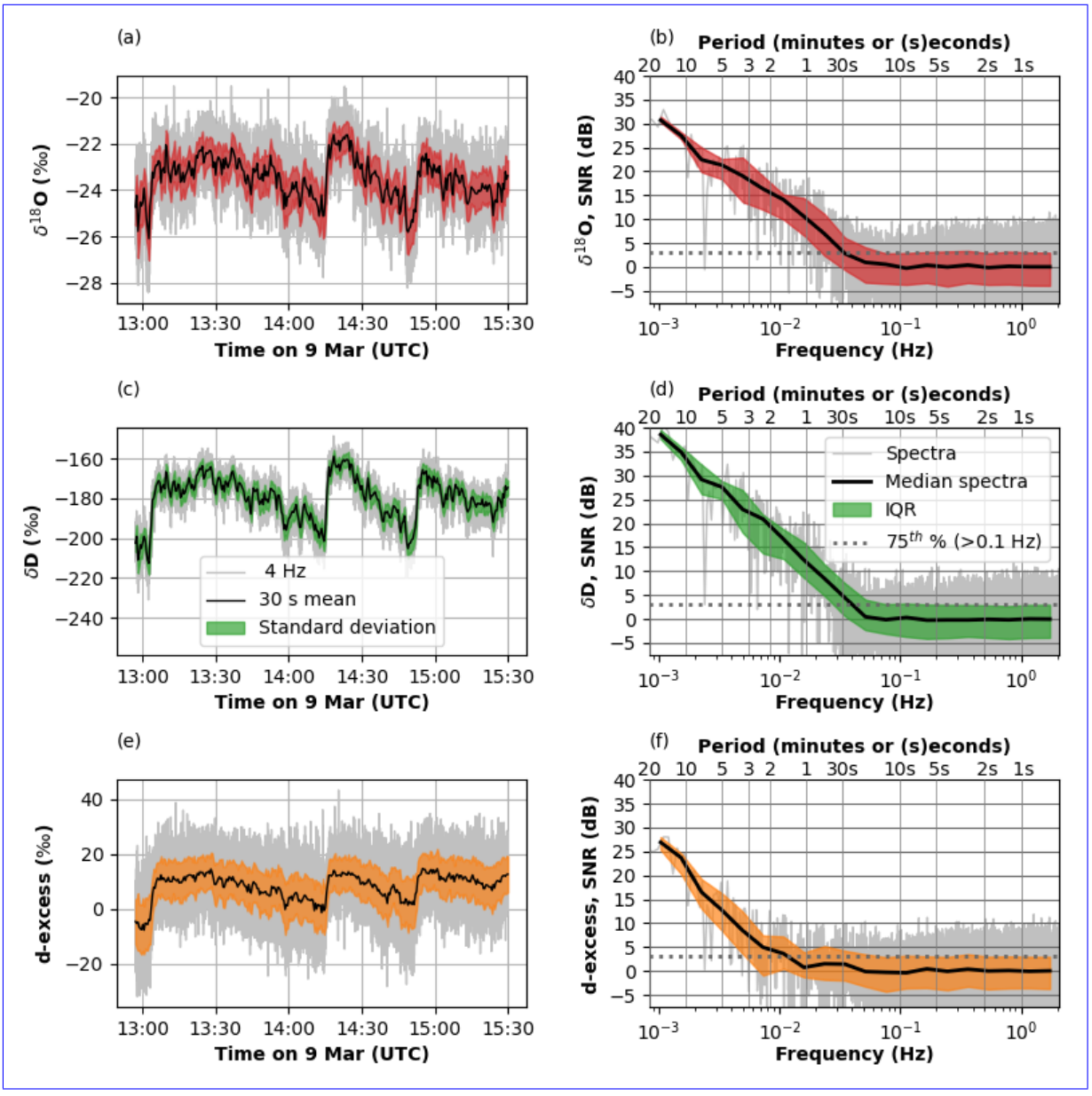


**Figure 9.** Resolving isotopic signals during the profiling period on 9 Mar 2020, from 12:57 to 15:30 UTC. (a) The 4 Hz $\delta^{18}$O signal (gray), with the 30 s mean (thick black) and standard deviation of the same (colored shading). (b) The fast Fourier transform of $\delta^{18}$O (gray), expressed as a signal to noise ratio. Black line is the median of the resulting power spectra, across 20 logarithmically spaced bins between between $8.33 \times 10^{-4}$ and 2 Hz, while colored shading is the interquartile range (IQR) of the bin. (c,d) Same as a,b), but for $\delta$D. (e,f) Same as a,b), but for d-excess.

**Table 4.**

| Time span | Isotope | Integrated Vapor (‰) | Collected Sample (‰) | Difference (‰) |
|---|---|---|---|---|
| 2020-02-25 15:20:00 to | $\delta^{18}$O | $-34.07 \pm 0.87$ | $-33.89 \pm 0.08$ | $0.18 \pm 0.87$ |
| 2020-02-26 08:50:00 | $\delta$D | $-274.6 \pm 1.2$ | $-244.5 \pm 0.4$ | $30.1 \pm 1.3$ |
| 2020-03-08 17:25:00 to | $\delta^{18}$O | $-27.10 \pm 0.87$ | $-25.90 \pm 0.07$ | $1.20 \pm 0.87$ |
| 2020-03-09 08:20:00 | $\delta$D | $-220.0 \pm 1.2$ | $-193.7 \pm 0.4$ | $26.3 \pm 1.3$ |

humid Snow site, the median SNR is equal to or above 5 dB after 4 minutes (see Supplemental Material). Therefore, across both deployment sites, we determine that maintaining a single height for at least 4 minutes is necessary to begin to resolve the signal during profiling, though longer durations will yield a higher resolving power.

### 4.4 Cold Trap module performance

The Cold Trap expansion module was fully integrated into the sample air flow of the ISE-CUBE system during the field tests. Since the Cold Trap box was not thermally regulated, the cryocooler unit was operated well below the manufacturers minimum operating guideline of 5 °C, reaching −5 °C over sustained periods, and even down to −20 °C occasionally. Nonetheless, the cryocooler reliably provided temperatures of $-80 \pm 5$ °C at the base of the vial enclosure for 80 % of the deployment. The remaining 20 % mostly occurred during overnight collections, whereby excessive frost buildup on the exterior of the brass vial enclosure would provide additional insulation and the vial temperature would drop below −85 °C. ~~Regardless, water~~ Vapor collection in a vial lasted between 8 hours and 16 hours during daytime and nighttime, with target flow rates of 0.5 L min$^{-1}$ and 0.25 L min$^{-1}$, respectively. Water vapor was successfully collected during a total of 28 periods, with up to 0.3 mL in a single sample~~. Vapor collection in a vial lasted between 8 hours and 16 hours during daytime and nighttime, with target flow rates of 0.5 L min$^{-1}$ and 0.25 L min$^{-1}$, respectively. However,~~ , though some samples collected significantly less.

We now present a comparison between two collected samples and the mass-flow integrated isotope measurements from the analyzer (Table 4). One sample is from during the Snow deployment, while the other is from the time at the Fjord. While $\delta^{18}$O values are close to being within measurement error, the $\delta$D values are quite different. This is likely due to a combination of deficiencies involving sample collection, inconsistent flow regulation, and possibly kinetic fractionation effects. These kinetic fractionation effects might arise from incomplete freeze out of the vapor, due to insufficient thermal stability of the glass sample vial. We additionally observed substantial ice crystal formation in the neck of the collection vials, which inhibited and decreased flow during multiple collection periods. This ice formation also compromised sample recovery during vial exchange, causing frozen sample to fall out of the vial during collection. These deficiencies could be corrected with a different collection vial and a better flow regulator (i.e. a mass flow controller), although sample analysis procedure would need to be changed.

In summary, we provide here a first proof-of-concept that a cryocooler-based Cold Trap module can be integrated into the ISE-CUBE system. Remaining shortcomings of the design can be rectified in future module iterations. A more detailed evaluation of the performance of the Cold Trap module in terms of sampling efficiency and its ~~use~~ suitability for in-field calibration is however beyond the scope of this manuscript and will be detailed in a future publication.

~~Comparison between temperature sensor of automated weather station ($T_{AWS}$) and the inlet temperature sensor ($T_{head}$). Both were at a height of 100 cm above the surface of the snow for 37 hours. Solid gray line represents 1-to-1 ratio. Dotted line indicates linear regressions through the data points, with purple shading (barely visible under dotted line) shows the 95 % confidence interval.~~

### 4.5 ~~Profiling module performance~~Example of a profiling operation

~~The Profiling expansion of the ISE-CUBE system can be evaluated in terms of the response time for mixing ratio and isotope measurements. With the heated tubing from inlet tip to the inlet of the analyzer and a diameter of 4.5 mm at a flow rate of about 9 L min$^{-1}$ in the Profiling module tubing, and 0.15 L min$^{-1}$ in the manifold tubing, the minimum response time would be approximately 6 s. However, estimates from the field show the actual response time of the analyzer to a humidity change to be 13 to 18 sec. Following the approach of Steen-Larsen et al. (2014b) and Wahl et al. (2021), a fast Fourier transform analysis documented a practical minimum averaging time of approximate 30 s due to wall effects in the tubing and analyzer causing increased memory effect. More detailed evaluation of the response of the inlet is currently precluded by the lack of asuitable device to produce a defined vapor isotope stream at sufficiently high flow rates.~~

~~In addition,~~ We now present an example for a profiling operation at the ~~auxiliary measurements from the ultrasonic distance sensor and the temperature probe at the tip of the inlet can be evaluated. The distance given by the ultrasonic sensor was periodically checked against a manual tape measure throughout the field deployment (accuracy ±~2 cm) . The behavior of the ultrasonic sensor did vary between the two measurements sites, likely as a result of underlying surface. While deployed over snow,~~ Fjord site on the afternoon of 9 Mar 2020, from 12:57 to 15:30 (UTC). Winds during this period were fairly constant around 7 m s$^{-1}$, occasionally gusting to 9 m s$^{-1}$. The entire profiling operation consisted of a sequence of 19 steps across three cycles, performed at heights between 1.5 m and 3.5 m above the surface of the water (Figure 10a, black line). The profiling head was kept at any particular height for 4.5 to 13 minutes (Figure 10a, yellow highlights), with the first 30 s at the level disregarded. Throughout the profiling operation, air temperature at the ~~sensor functioned with 2 cm accuracy over the range of 50 to 205 cm. When the inlet head was lowered below 50 cm, the sensor gave unreliable and clearly spurious measurements. We speculate that the particular type of ultrasonic sensor used was affected by the acoustic properties of the snowpack below this threshold. In these circumstances, manual distance was taken with a tape measure, with corresponding markings made on the controlling steel cable~~ inlet and specific humidity were anti-correlated with height (Figure 10a, cyan and blue lines, respectively). Across the 2 m profile span, a linear fit through the observed humidities yielded a gradient (with 95% confidence interval) of $-0.13 \pm 0.04$ g/kg/m (Figure 10b, blue). The linear fit for air temperature was $-0.63 \pm 0.17$ K/m (Figure 10b, cyan). This was to be expected, as the surface of the water was a source of both heat and moisture.

The isotopic signature of the moisture also exhibited a gradient. $\delta^{18}$O, $\delta$D, and the d-excess (Figure ~~2)~~ 10c,d,e) all display negative gradients across their linear fits ($-0.86 \pm 0.49$ ‰/m, $-13.4 \pm 5.3$ ‰/m, and $-6.52 \pm 2.17$ ‰/m, respectively). Even with the increased uncertainty established in Sect. 4.2 accounted for and in addition to the standard errors of the measurement means (99 % confidence interval) (Figure 10c,d,e; errorbars), the gradients are well-resolved, and have a narrow 95 % confidence interval (Figure 10b-e; blacking shading). ~~No issues with distance sensors were encountered while deployed~~

at the Fjord location with water or sea ice at the surface.At both locations, a low signal to noise ratio and a jumpy distance signal was observed during strong winds ($>11\,\mathrm{m\,s^{-1}}$) , possibly due to the ultrasonic pulse being advected away before the reflected signal was received.

Finally, the temperature sensor above the tip of the inlet of the profiling module was compared against the temperature sensor of an automated weather station (Jocher et al., 2012; Schulz, 2017) ($20\,\mathrm{m}$ away) at a height of $100\,\mathrm{cm}$ for $37\,\mathrm{hours}$ (during 25 Feb and 26 Feb). The minutely averaged temperature records of the two sensors show a high correlation of 0.991, with a linear regression slope of $1.000 \pm 0.005$ (Figure E1). The profiling sensor consistently recorded higher temperatures than the AWS, having a linear regression offset of $0.6\,^{\circ}\mathrm{C}$. While distance between sensors might account for some of this discrepancy, the gradients observed with the Profiling module are almost an order of magnitude larger, with relative changes well captured due to the high linearity. Overall, the Profiling Module functioned reliably, guiding ambient air to the analyzer with a response time for water vapor step changes within 13 to 18 sec.

### 4.6 Example of a profiling operation

We now present an example for a profiling operation in the surface layer during strongly stable conditions, performed at heights between $0.04\,\mathrm{m}$ and $2.00\,\mathrm{m}$ above snow on the morning of 28 Feb 2020. The entire profiling operation consisted of a sequence of 6 steps between the lowest level at $0.04\,\mathrm{m}$, progressing to $2.00\,\mathrm{m}$, with about 5 min time intervals (Figure 10a , black bars). The specific humidity during this upward profile increased from $0.25\,\mathrm{g\,kg^{-1}}$ at the lowest level, to $0.4\,\mathrm{g\,kg^{-1}}$ at $1.50\,\mathrm{m}$ and above (Figure 10a, blue dashed). The calibrated isotope species showed the strongest gradients in the lowest $1\,\mathrm{m}$ above the surface, with $-0.5\,‰/\mathrm{m}$ and $17\,‰/\mathrm{m}$ respectively.

After working through the upwards stepping of our profile, we further probed the substantial moisture gradient with first a large $1\,\mathrm{m}$ step down, from $150\,\mathrm{cm}$ to $50\,\mathrm{cm}$ (Figure 10a ). As we expected, this step down resulted in a drop in specific humidity; it again rose when height was increased to $120\,\mathrm{cm}$. During further narrowing iterations, we probed near the height of the strongest moisture gradient in the surface layer. Simultaneously, we captured isotope signature of $\delta^{18}$O and $\delta$D (Figure 10b). At

## 5 Discussion

With the ability to resolve near-surface profiles, the ISE-CUBE system offers a number of advantages over a valve/manifold combination. Fundamentally, the profiling arm allows for increased continuity in the observed profiles, as compared to a fixed height tower. The freedom to chose any height in the $2\,\mathrm{m}$ range enabled us to produce fine-scale vertical profiles with a resolution of approximately $25\,\mathrm{cm}$. Though this particular interval is arbitrary, being able to select heights of interest while measuring led to a more dynamic sampling strategy that could be adapted on-the-fly. Duplicating a profile such as obtained on 9 :07 there was a sudden veering of the winds (S to SW), followed by a backing (SW to ESE)(Figure 10e). The veering was also associated with an increase in wind speed, and the development of shear in the lowermost meter (Figure 10d).In addition, the already present temperature gradient strengthened further (Figure 10e). From 9:30 until 9:55, the temperature gradient between

~~the two heights (250 to 100 cm and 100 to 50 cm) converged as observed with continuing profiling operations. Ultimately, after profile completion at 9:55, we left the inlet head at a static height of 75 cm for some hours (not shown), in an effort to observe any oscillations moving through the interface.Duplicating such a process with a valve~~Mar would involve an approximate eightfold increase in the number of inlet lines, without any guarantee that an inlet would be at a height of interest. Unlike typical tower measurements, the short inlet lines of the Profiling module allow for rapid instrument response, and limit potential wall interactions with the tubing during sample transmission. These short inlet lines are only possible due to the relatively small size of the ISE-CUBE stack (as compared to previous, larger enclosures) and the thin silhouette of the Profiling frame, which limits flow distortion. In addition, the flexibility of the measurement height with the articulating arm is a clear asset for measurements over water surface with strong tidal variation. Finally, it would be quite possible to deploy alongside tower and valve/~~manifold system in~~ manifold combinations, thus supplementing high-resolution vertical profiles in the lowermost surface layer with sampling across a larger height range. A measurement strategy like this would provide information on the rapidly occurring surface processes alongside the more continuous context they are take place under.

Speculation on such a measurement strategy might imply that the ISE-CUBEs could be deployed for longer periods. However this prototype has a practical time limitation imposed by calibration necessity. Currently, the integrated Cold trap is unsuitable to be used for calibrating CRDS measurements. However, if one could integrate a field calibration module into the system, the system could very likely stand on its own for extended periods of time. While the Analyzer and Pump modules could used without the Profiling module for an extended deployment, at some point one would start to reach a point of diminishing returns. A larger, more conventional enclosure offers a level of security that the ISE-CUBEs cannot provide for long-term measurement efforts that are less concerned with small scale processes; small scale processes which do not necessarily require a long deployment to observe.

Regardless of deployment length, the ~~surface layer would involve at least a tripling of inlet tubing, yet without guarantee that any given inlet would be at a height of interest.~~ current ISE-CUBE system is limited by the lack of an active temperature control capability, which presently prevents operation in warmer measurement environments. With the modular approach, the addition of a dedicated ventilation module with larger fans and active cooling/heating unit is straightforward, and would enable deployment in warmer and more variable climatic conditions. Preliminary testing with such a module has already yielded promising results in ambient temperatures up to around 20 °C, though shielded from direct sunlight (see Supplemental material).

One potential internal change in our measurement setup would involve the high flow mode described in Sect. 2.2. This mode enabled 4 Hz sampling and enhanced instrument response time. However, it is unexplored if the measurement precisions found in Sect. 4.2 might be improved if the instrument were to remain in standard low-flow mode. Were this the case, the inlet assembly would need to be modified to even further reduce the amount of tubing subjected to this decreased flow and maintain most rapid instrument response.

## 6 Conclusions and Outlook

In this work, we have detailed the design and performance of the new ISE-CUBE system for ~~in-situ~~ near-surface profiles of water vapor isotope measurements. ~~The ISE-CUBE system is a modular field-going deployment system for in-situ laser-based spectroscopy. The modular~~ The modular design enables rapid installation, while the compact system size provides minimized flow distortion around the measurement site~~. We apply the system and evaluate its performance for the specific case of stable isotope measurements of water vapor in the lowermost 2 m of the atmosphere in an Arctic environment.~~ , and allows us to measure in stable conditions with shallow boundary layer.

During a two-week long field ~~deployment at~~ experiment in Ny-Ålesund, Svalbard, Norway during Feb–Mar 2020, the analyzer encountered extreme ~~ambient winds and temperatures. While~~ environmental conditions while deployed in the system. Though ambient temperatures reached down to $-30\,^{\circ}\mathrm{C}$, ~~and winds were gusting to over $20\,\mathrm{m\,s^{-1}}$,~~ the analyzer remained within its specified range of measurement conditions with regard to ~~$T_C$, $T_{WB}$, $T_{DAS}$, and $p_C$~~ $T_C$, $T_{WB}$, $T_{DAS}$, and $p_C$. Measurement precisions during the field deployment were on average ~~0.06 ‰~~ 0.10 ‰ ($\delta^{18}$O) and ~~0.47 ‰~~ 0.93 ‰ ($\delta$D) lower than in the ~~laboratory benchmark, irrespective of ambient mixing ratios. Our results demonstrate that the ISE-CUBE system allows for in-situ CRDS measurements in harsh environments that are only marginally less precise than measurements in a laboratory environment.~~ reference benchmarks.

The profiling ~~expansion~~ module, a height-adjustable sampling arm ~~within the range of 0 to 2 m above the surface, enabled flexible and sufficiently precise~~ with a range of 2 m, enabled profiling of the water isotope composition throughout the ~~surface layer~~shallow surface layer in a stable atmosphere. With a response time of ~~about 13 to 18 sec, giving a minimum averaging time of 30 s,~~ approximately 20 sec, the ISE-CUBE system captured profiles and gradients in ~~the strongly stratified stable boundary layer. In addition, the flexibility of the measurement height was a clear asset for measurements over water surface with strong tides. Additionally, combinations with tower and manifold systems are also possible, thus supplementing high-resolution vertical profiles in the surface layer with sampling across a larger height range~~this layer. Even at the low humidities (down to 0.25 g/kg) over the tundra, the profiles achieve a high enough signal to noise ratio to resolve the vertical isotopic gradients after approximately 4 minutes at each height interval. Due to the high vertical resolution in the profiles, the robustness of the observed gradient is high.

Integration of the Cold-Trapping expansion module based on the design of ~~Peters and Yakir~~ Peters and Yakir (2010) into the ISE-CUBE system enabled quantitative vapor collection. Samples were typically collected over a duration of 8 hours or more in low-humidity environments, resulting in a maximum collection of 0.3 mL at a time. Such cold-trapping enables subsequent liquid sample analysis in a laboratory environment for quality control of the calibration, and the measurement of $H_2^{17}O$ for triple-isotope capability. While the cold trap module is functional, ~~additional evaluation of the sampling efficiency, and design optimizations to facilitate sample handling are needed~~the preliminary results provided here show that design refinements are necessary.

The ~~next expansion~~modular nature of the system invites additional expansion. A top-priority expansion module would focus on an in-field calibration system. In general, there are multiple potential calibration devices using a variety of vapor generation

methods (Iannone et al., 2009; Gkinis et al., 2010; Ellehoj et al., 2013); the device just needs to be robust and suitably compact, all while generating a consistent source of known vapor. For example, Leroy-Dos Santos et al. (2021) have put forward an instrument that can generate stable vapor streams down to ~~70 ppmv~~0.045 g/kg (70 ppmv), one of which has been operating mostly autonomously in Antarctica, with little manual intervention. ~~Ultimately, when integrating a future calibration module into the system, the most important considerations are for the research aims and logistical limitations of the deployment itself.~~ Further potential expansion modules include a Battery power module which would permit mobile operation. In addition to an enhanced Ventilation module, an enhanced, automonous Profiling module would remove the need for nearby operators, removing any chance of human-induced error in the stable water isotope measurements.

~~One current limitation of the ISE-CUBE system is the lack of an active temperature control capability, which presently prevents operationin warmer measurement environments. With the modular approach, the addition of a dedicated ventilation modulewith larger fans and active cooling~~Deployments need not be limited to measurements of stable water isotopes. Many laser spectrometers for other atmospheric trace gases, such as methane, carbon dioxide, or carbon isotopes may be integrated into the system and used for purposes beyond meteorology/~~heating unit is straightforward, and would enable deployment in warmer and more variable climatic conditions. An additional battery power module would permit mobile operation for limited time periods, thus allowing for the study of spatial variability.~~

~~The availability of a modular, versatile deployment system such as the ISE-CUBEs implies easy access to remote locations and environments, while maintaining necessary data quality standards. Locations~~ hydrology; those produced by Picarro would most readily fit the system, but are not limited to. With a more robust temperature controller, there is the possibility for deployment in more temperate environments. Such locations may include, but are not limited to, glaciers, sea ice, lakes, coastal areas, caves, forests, grasslands, croplands, deserts, and other places where evaporation and condensation interactions with the surface contribute to the vapor isotope composition of the near-surface atmosphere. ~~The limited footprint and robust handling also allows for installation on open moving platforms to obtain spatial transects. Finally, laser spectrometers for other atmospheric trace gases, such as methane, carbon dioxide, or carbon isotopes may be integrated into the system~~

The availability of a modular, versatile deployment system such as the ISE-CUBEs implies easy access to remote locations and environments, while maintaining necessary data quality standards. As we provide the design in a easily reproducible way to the community (see Supplemental Material), we endeavor to enable further development and widespread acquisition of high-quality datasets from previously inaccessible measurement locations.

~~30 s averaged timeseries of profiling operations, alongside ambient wind and temperature conditions from the morning of 28 Feb 2020. (a) Inlet head height (above surface of the snow; solid black) and specific humidity (dashed blue). Shading denotes 1-$\sigma$. (b) $\delta^{18}$O (solid blue) and $\delta$D (dashed black). Shading denotes 1-$\sigma$. (c) Wind direction: 250 cm = upwards triangles; 100 cm = circles; and 50 cm = downwards triangles. (d) Wind speed (left axis, colored): 250 cm = solid colored lines; 100 cm = dashed colored lines; and 50 cm = dotted colored lines. Wind shear (right axis, black): 250 – 100 cm = black dashed lines; and 100 – 50 cm = black dotted lines. (e) Temperature (left axis, colored): 250 cm = solid colored lines; 100 cm = dashed colored lines; and 50 cm = dotted colored lines. Temperature gradient (right axis, black): 250 – 100 cm = black dashed lines; and 100 – 50 cm = black dotted lines.~~

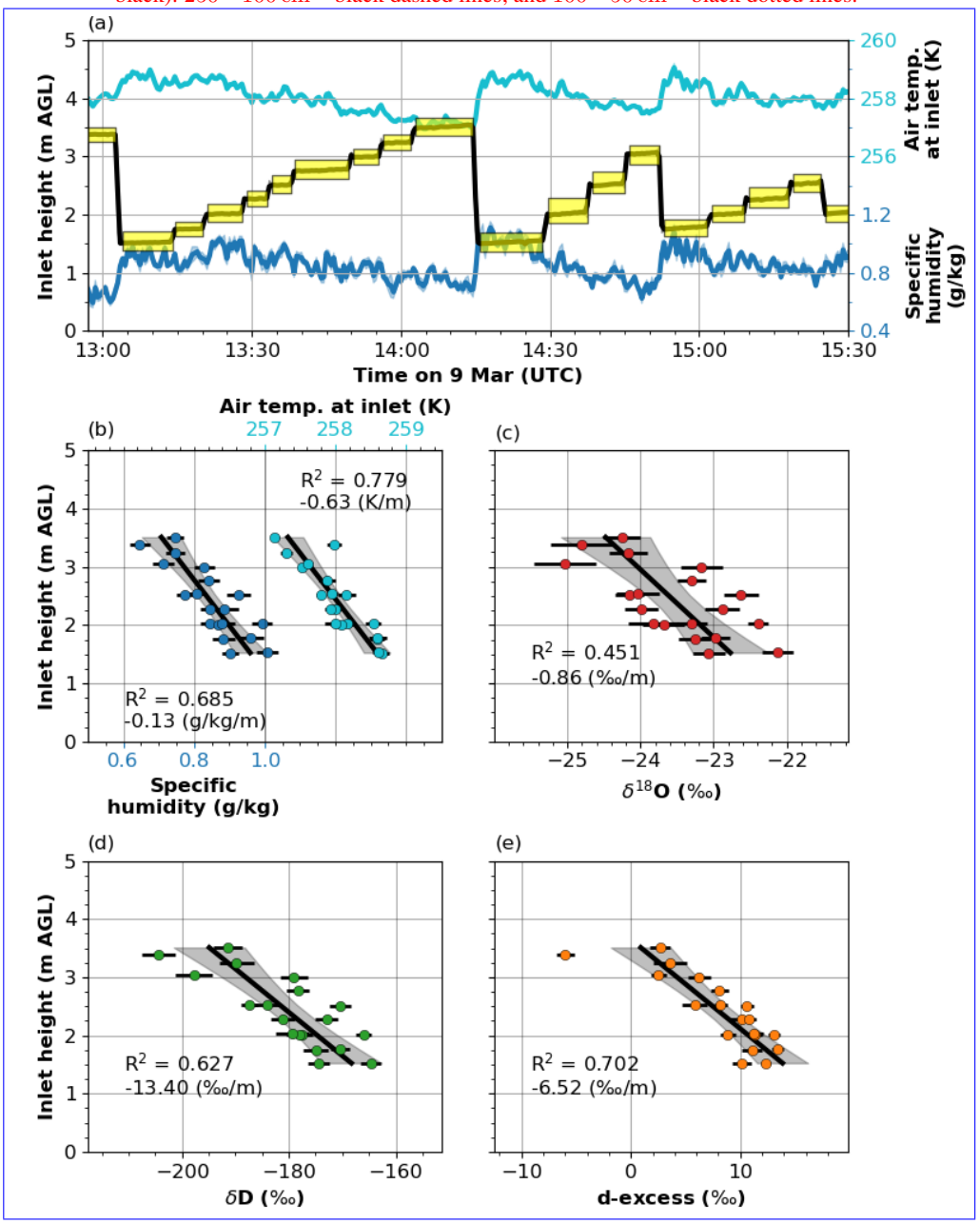


**Figure 10.** A profiling operation from 12:57 to 15:30 on 9 Mar 2020. (a) A time series of inlet head height (black lines, left axis), alongside the air temperature at the same (cyan line, upper right axis) and specific humidity (blue line, lower right axis). 19 height levels and their durations denoted with yellow highlighting. (b) Vertical profiles of the air temperature at the inlet head (cyan, upper-right axis) and specific humidity (blue, bottom-left axis). Errorbars indicate standard errors, with 99 % confidence interval. Standard errors also include increased

## Appendix A: ISE-CUBE component list

**Table A1.** Components used in the ISE-CUBE system. General ~~pneumatic~~ gas connections (PTFE tubing, unions, reducers, etc.) made with parts from Swagelok Inc. Files for 3D printed ventilation mounts were custom-made and not listed (see Supplemental Material). Modular abbreviations: AN=Analyzer module; PU=Pump module; CT=Cold Trap module; PR=Profiling module.

| Module | Component | Manufacturer | Model/Series | Size(LxWxH); Weight; Detail |
|---|---|---|---|---|
| AN/PU/CT | Module container | Pelican Products Inc. | iM2875 Storm | 632 x 602 x 333 mm; 9.1 kg |
| AN | CRDS analyser | Picarro Inc. | L-2130i | 20.4 kg; 230 VAC |
| AN/PU | Reinforced PVC vacuum tubing | Kuriyama of America Inc. | K7160-06 | 3/8 inch |
| PU | CRDS vacuum pump | KNF DAC GmbH | N920AP.29.18 | 10.5 kg; 230 VAC |
| PU | Inlet vacuum pump | KNF DAC GmbH | N022AN.18 | 4.0 kg; 230 VAC |
| PU | UPS | Eaton | EL500FR | 2.9 kg; 230 VAC |
| CT | Cryocooler | Sunpower Inc. | Cryotel MT | 2.1 kg; 24 VDC |
| CT | Collection vial | ThermoSci | 2-SVW Chromacol | 2 mL |
| CT | UPS | Phoenix Contact | 2866611 | 5.6 kg; 24 VDC |
| CT | 12 VDC (out) power supply | Mean Well | DDR-15G-12 | 9 to 36 VDC input |
| CT | Flow meter | Sierra Instruments Inc. | TopTrak 822 | 12 VDC; 0-1 ~~&~~ and 0-30 $\mathrm{L\,min^{-1}}$ |
| AN/PU/CT | Ventilation fan | ebm-papst GmbH & Co. KG | RL 90 | 0.7 kg; 230 VAC |
| AN/PU/CT | Protective cover | IKEA | TOSTERÖ | 1000 x 700 x 900 mm; 0.75 kg |
| AN/PU/CT | Power connector | Amphenol | 62GB | 230 VAC |
| AN | Data connector | Amphenol | RJ45F7RJ | RJ45 |
| AN/CT | Data connector | RS Pro | 111-6759 | USB |
| AN/PU/CT | Inlet vacuum connector | Swagelok Inc. | SS-400-61 | 1/4 inch |
| AN/PU | Picarro vacuum connector | Swagelok Inc. | SS-600-61 | 3/8 inch |
| AN/PU | One-way check valve | Swagelok Inc. | 6L-CW4S4 | 1/4 inch |
| PU/CT | Aluminium support frame | RatRig | V-Slot 2020 | |
| CT/PR | Microcontroller | Arduino | UNO ~~&~~ and Mega | 12 VDC |
| CT/PR | Temperature sensor | Velleman | VMA324 | $-55$ to 125 °C |
| PR | Ultrasonic distance sensor | SparkFun Elec. | SEN-15569 (HC-SR04) | 0 to 5 m |
| PR | Module Container | Pelican Products Inc. | 1120 | 214 x 172 x 98 mm; 0.6 kg |
| PR | Inlet heat trace | Thermon Inc. | BSX 10-2 | 60 °C; 32 W/m |
| PR | Aluminium tripod | Campbell Scientific | CM110 | 15 kg |
| PR | Hand winch | Hamron | - | 350 kg rating |
| AN/PU/CT | AC mains power cable | Lapp | 0013631 | 3-core; 230 V; $-40$ °C rating |
| PU/PR | DC power ~~&~~ and signal cable | Alpha Wire EcoFlex | 79002 SL005 | 3-core; 12 V; $-40$ °C rating |

## Appendix B: Campaign location

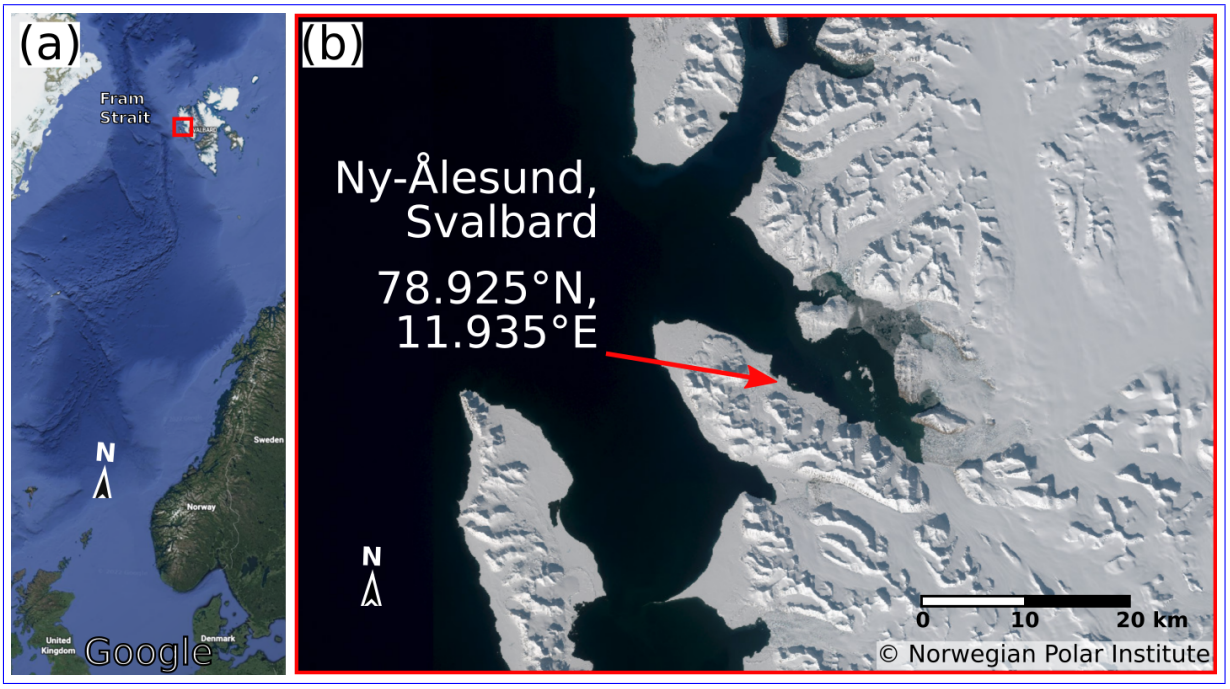


**Figure B1.** (a) Location of Svalbard and campaign area (red square) (© Google Earth 2022). (b) Zoom in on campaign area showing the location of Ny-Ålesund on the southern shore of Kongsfjorden (© Norwegian Polar Institute, http://toposvalbard.npolar.no).

## Appendix C: ~~$T_{DAS}$~~ $T_{DAS}$ and ~~$T_{WB}$~~ $T_{WB}$ relationship

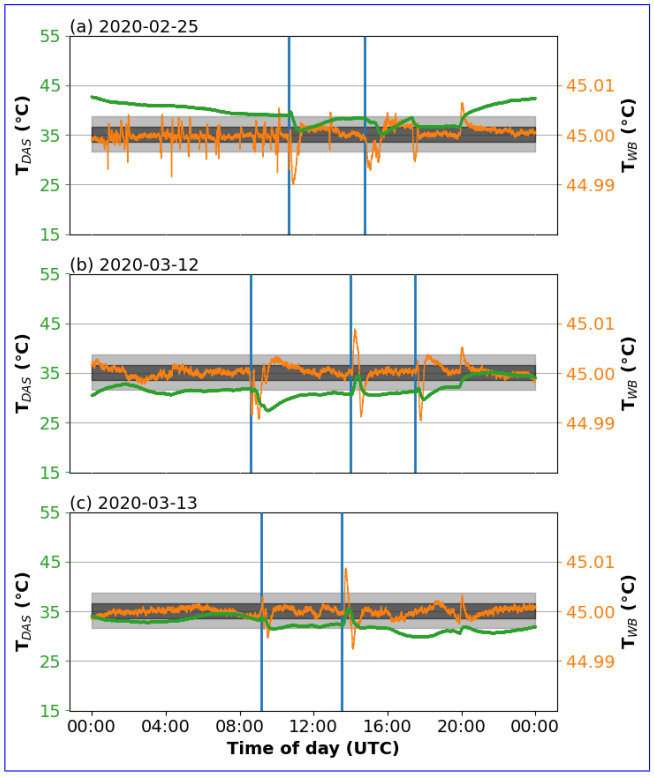


**Figure C1.** Daily timeseries of DAS temperature (left axis, green) and Warm Box temperature (right axis, orange) on (a) 25 Feb 2020, (b) 12 Mar 2020, and (c) 13 Mar 2020. Black shading denotes spread between 2nd and 98th percentiles of Warm Box temperatures during laboratory benchmark. Gray shading indicates the same, for the ~~time~~ deployment period in the Zeppelin Observatory. Blue lines are brief site visits, lasting on the order of 5 to 10 minutes.

Increases or decreases in ~~$T_{DAS}$~~ $T_{DAS}$ had a tendency to ~~initiate~~ coincide with sudden dips or spikes in ~~$T_{WB}$~~ $T_{WB}$ (Figures C1 ~~&~~and C2). While the impact of ~~$T_{DAS}$~~ $T_{DAS}$ perturbations could last up to around 4 hours, ~~$T_{WB}$~~ $T_{WB}$ instability was shorter lived, usually returning to benchmark values within an hour. However, the magnitude of these perturbations, and the subsequent recovery time, is largely related to the kind of operation prompting the disturbance. Brief ~~operations~~ site visits (Figure C1, blue lines), such as routine checks or swapping Cold Trap collection vials, would produce a relatively small change in ~~$T_{DAS}$~~ $T_{DAS}$, as compared to longer operations (Figure C2, blue shading), such as profiling. Accordingly, recovery time for the ~~$T_{WB}$~~ $T_{WB}$ would also be longer during the profiling periods, though the magnitude of the ~~$T_{WB}$~~ $T_{WB}$ dip/spike ~~could be comparable across all operations~~is independent of site visit type.

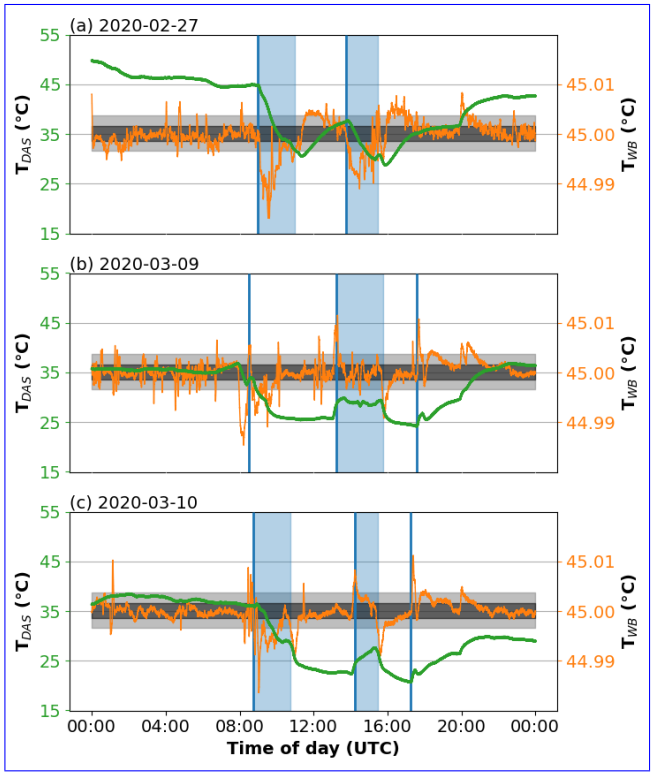


**Figure C2.** Similar to Figure C1, but for (a) 27 Feb 2020, (b) 9 Mar 2020, and (c) 10 Mar 2020. Blue shading indicates profiling periods, where the ISE-CUBEs were attended with the cover removed.

## Appendix D: ~~WLM metrics between field and observatory~~

~~(a) Baseline Shift, (b) Slope Shift, and (c) Residuals of the expected model spectrum versus the fitted absorption spectrum from the analyzer's WLM. Light gray line represents 1-to-1 ratio. Data are divided into 300 ppmv bins, from 300 to 3900 ppmv (colorbar), with error bars denoting IQR for both Zeppelin observatory and field measurements. Dotted lines indicate linear regressions through the data points, with gray shading showing the 95 % confidence interval.~~

## Appendix D: Laboratory benchmark sequences

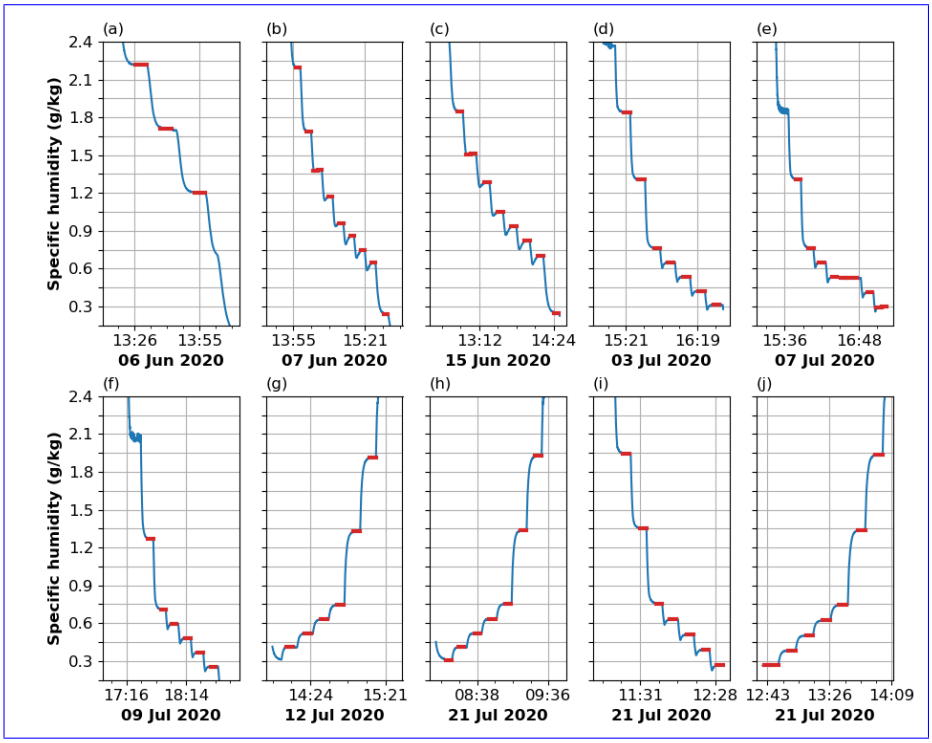


**Figure D1.** Humidity step sequences from ~~eight~~ ten (~~a~~ha-j) distinct usage events from laboratory characterization of the analyzer, during the period of June to July 2020. Blue line depicts volumetric mixing ratio, with red highlights showing ~~the most stable~~ 5 minute periods ~~within each mixing ratio bin~~with a standard deviation less than 0.006 g/kg. (a-c) used 100 % nitrogen as carrier gas, while (d-j) used synthetic air (80 % $N_2$, 20 % $O_2$). All events used a lab standard of a similar depletion ($\delta^{18}O$: $-40.02 \pm 0.07$‰ and $\delta D$: $-307.8 \pm 0.8$‰) as measured in the field.

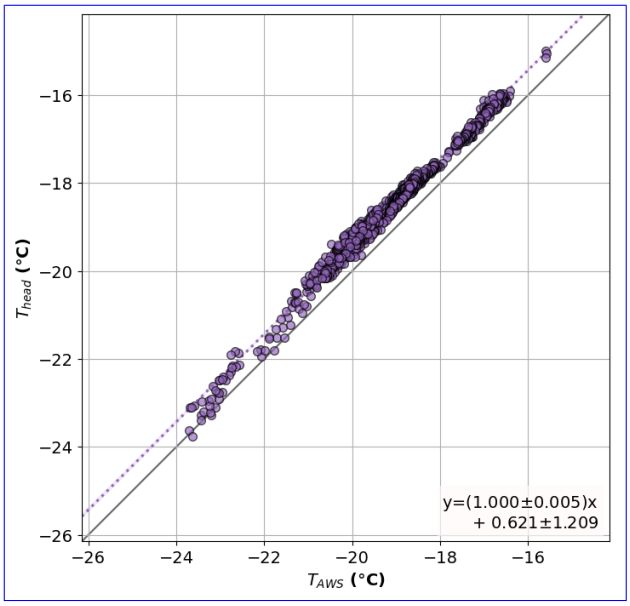


**Figure E1.** Comparison between temperature sensor of automated weather station ($T_{AWS}$) and the inlet temperature sensor ($T_{head}$). Both were at a height of 100 cm above the surface of the snow for 37 hours. Solid gray line represents 1-to-1 ratio. Dotted line indicates linear regressions through the data points, with purple shading (barely visible under dotted line) shows the 95 % confidence interval.

## Appendix E: Profiling module sensor performance

The distance given by the ultrasonic sensor was periodically checked against a manual tape measure throughout the field deployment (accuracy $\pm\sim$2 cm). The behavior of the ultrasonic sensor did vary between the two measurements sites, likely as a result of underlying surface. While deployed over snow, the sensor functioned with 2 cm accuracy over the range of 50 to 205 cm. When the inlet head was lowered below 50 cm, the sensor gave unreliable and clearly spurious measurements. We speculate that the particular type of ultrasonic sensor used was affected by the acoustic properties of the snowpack below this threshold. In these circumstances, manual distance was taken with a tape measure, with corresponding markings made on the controlling steel cable. No issues with distance sensors were encountered while deployed at the Fjord location with water or sea ice at the surface. At both locations, we observed a low signal to noise ratio (SNR) and a jumpy distance signal during strong winds ($>$11 m s$^{-1}$), possibly due to the ultrasonic pulse being advected away before the reflected signal was received.

The temperature sensor above the tip of the inlet of the profiling module was compared against the temperature sensor of an automated weather station (Jocher et al., 2012; Schulz, 2017) (20 m away) at a height of 100 cm for 37 hours (during 25 Feb and 26 Feb). The 1-minute averaged temperature records of the two sensors show a high correlation of 0.991, with a linear regression slope of 1.000 $\pm$ 0.005 (Figure E1). The profiling sensor consistently recorded higher temperatures than the AWS, having a linear regression offset of 0.6 °C. While distance between sensors might account for some of this discrepancy, the

gradients observed with the Profiling module are almost an order of magnitude larger, with relative changes well captured due to the high linearity. Overall, the sensors installed on the Profiling module functioned adequately.

*Author contributions.* Conceptualization (design): AS, HS, HCSL; Methodology (construction): AS, HS; Investigation: AS, HS; Formal analysis: AS, HS; Writing – original draft preparation: AS; Writing – review and editing: All authors

*Competing interests.* The authors declare no conflict of interest. The funders had no role in the design of the study; in the collection, analyses, or interpretation of data; in the writing of the manuscript, or in the decision to publish the results.

*Acknowledgements.* The authors wish to acknowledge: Anak Bhandari, Helge Bryhni, ~~&~~ and Tor de Lange for their technical expertise during the construction process; Alexander Schulz for the data from the AWI Ny-Ålesund eddy-covariance meteorological station; ~~and~~ Aina Johannessen, Alena Dekhtyareva, ~~&~~ and Marius Jonassen for their invaluable roles in the ISLAS2020 campaign; Daniele Zannoni for his suggestions and help concerning the inlet response analysis; and Ove Hermansen for access to Zeppelin Observatory. The authors also wish to make a special acknowledgment to the memory of Leon Isaac Peters for his incredibly patient and ~~helpful~~ supportive insights regarding the ~~Cold Trap Module~~design of the Cold Trap module. This work has been funded by the European Research Council (Consolidator Grant ISLAS, project. 773245).

## References


Aemisegger, F., Sturm, P., Graf, P., Sodemann, H., Pfahl, S., Knohl, A., and Wernli, H.: Measuring variations of $\delta$18O and $\delta$2H in atmospheric water vapour using two commercial laser-based spectrometers: an instrument characterisation study, Atmospheric Measurement Techniques, 5, 1491–1511, https://doi.org/10.5194/amt-5-1491-2012, https://amt.copernicus.org/articles/5/1491/2012/, 2012.

Berkelhammer, M., Noone, D. C., Steen-Larsen, H. C., Bailey, A., Cox, C. J., O'Neill, M. S., Schneider, D., Steffen, K., and White, J. W.: Surface-atmosphere decoupling limits accumulation at Summit, Greenland, Science Advances, 2, 1–10, https://doi.org/10.1126/sciadv.1501704, 2016.

Bonne, J. L., Masson-Delmotte, V., Cattani, O., Delmotte, M., Risi, C., Sodemann, H., and Steen-Larsen, H. C.: The isotopic composition of water vapour and precipitation in Ivittuut, southern Greenland, Atmospheric Chemistry and Physics, 14, 4419–4439, https://doi.org/10.5194/acp-14-4419-2014, 2014.

Chazette, P., Flamant, C., Sodemann, H., Totems, J., Monod, A., Dieudonné, E., Baron, A., Seidl, A., Steen-Larsen, H. C., Doira, P., Durand, A., and Ravier, S.: Experimental investigation of the stable water isotope distribution in an Alpine lake environment (L-WAIVE), Atmospheric Chemistry and Physics, 21, 10 911–10 937, https://doi.org/10.5194/acp-21-10911-2021, 2021.

Craig, H.: Isotopic Variations in Meteoric Waters, Science, 133, 1702–1703, 1961.

Crosson, E. R.: A cavity ring-down analyzer for measuring atmospheric levels of methane, carbon dioxide, and water vapor, Applied Physics B: Lasers and Optics, 92, 403–408, https://doi.org/10.1007/s00340-008-3135-y, 2008.

Crosson, E. R., Ricci, K. N., Richman, B. A., Chilese, F. C., Owano, T. G., Provencal, R. A., Todd, M. W., Glasser, J., Kachanov, A. A., Paldus, B. A., Spence, T. G., and Zare, R. N.: Stable Isotope Ratios Using Cavity Ring-Down Spectroscopy: Determination of 13C/12C for Carbon Dioxide in Human Breath, Analytical Chemistry, 74, 2003–2007, https://doi.org/10.1021/ac025511d, https://doi.org/10.1021/ac025511d, pMID: 12033299, 2002.

Dahlke, S., Solbès, A., and Maturilli, M.: Cold Air Outbreaks in Fram Strait: Climatology, Trends, and Observations During an Extreme Season in 2020, Journal of Geophysical Research: Atmospheres, 127, 1–18, https://doi.org/10.1029/2021JD035741, https://onlinelibrary.wiley.com/doi/10.1029/2021JD035741, 2022.

Dansgaard, W.: Stable isotopes in precipitation, Tellus, 16, 436–468, https://doi.org/10.3402/tellusa.v16i4.8993, https://www.tandfonline.com/doi/full/10.3402/tellusa.v16i4.8993, 1964.

Ellehoj, M. D., Steen-Larsen, H. C., Johnsen, S. J., and Madsen, M. B.: Ice-vapor equilibrium fractionation factor of hydrogen and oxygen isotopes: Experimental investigations and implications for stable water isotope studies, Rapid Communications in Mass Spectrometry, 27, 2149–2158, https://doi.org/10.1002/rcm.6668, http://doi.wiley.com/10.1002/rcm.6668, 2013.

Galewsky, J., Rella, C., Sharp, Z., Samuels, K., and Ward, D.: Surface measurements of upper tropospheric water vapor isotopic composition on the Chajnantor Plateau, Chile, Geophysical Research Letters, 38, 1–5, https://doi.org/10.1029/2011GL048557, 2011.

Galewsky, J., Steen-Larsen, H. C., Field, R. D., Worden, J., Risi, C., and Schneider, M.: Stable isotopes in atmospheric water vapor and applications to the hydrologic cycle, Reviews of Geophysics, 54, 809–865, https://doi.org/10.1002/2015RG000512, 2016.

Gkinis, V., Popp, T. J., Johnsen, S. J., and Blunier, T.: A continuous stream flash evaporator for the calibration of an IR cavity ring-down spectrometer for the isotopic analysis of water cavity ring-down spectrometer for the isotopic analysis of water, Isotopes in Environmental and Health Studies, 46, 463–475, https://doi.org/https://doi.org/10.1080/10256016.2010.538052, 2010.

Gupta, P., Noone, D., Galewsky, J., Sweeney, C., and Vaughn, B. H.: Demonstration of high-precision continuous measurements of water vapor isotopologues in laboratory and remote field deployments using wavelength-scanned cavity ring-down spectroscopy (WS-CRDS)

technology, Rapid Communications in Mass Spectrometry, 23, 2534–2542, https://doi.org/10.1002/rcm.4100, http://doi.wiley.com/10.1002/rcm.4100, 2009.

Iannone, R. Q., Romanini, D., Kassi, S., Meijer, H. A. J., and Kerstel, E.: A Microdrop Generator for the Calibration of a Water Vapor Isotope Ratio Spectrometer, Journal of Atmospheric and Oceanic Technology, 26, 1275–1288, https://doi.org/10.1175/2008JTECHA1218.1, 2009.

Jocher, G., Karner, F., Ritter, C., Neuber, R., Dethloff, K., Obleitner, F., Reuder, J., and Foken, T.: The Near-Surface Small-Scale Spatial and Temporal Variability of Sensible and Latent Heat Exchange in the Svalbard Region: A Case Study, ISRN Meteorology, 2012, 1–14, https://doi.org/10.5402/2012/357925, https://www.hindawi.com/journals/isrn/2012/357925/, 2012.

Johnson, J. E. and Rella, C. W.: Effects of variation in background mixing ratios of N2, O2, and Ar on the measurement of $\delta$18O–H2O and $\delta$2H–H2O values by cavity ring-down spectroscopy, Atmospheric Measurement Techniques, 10, 3073–3091, https://doi.org/10.5194/amt-10-3073-2017, https://amt.copernicus.org/articles/10/3073/2017/, 2017.

Kurita, N.: Origin of Arctic water vapor during the ice-growth season, Geophysical Research Letters, 38, 1–5, https://doi.org/10.1029/2010GL046064, 2011.

Leroy-Dos Santos, C., Casado, M., Prié, F., Jossoud, O., Kerstel, E., Farradèche, M., Kassi, S., Fourré, E., and Landais, A.: A dedicated robust instrument for water vapor generation at low humidity for use with a laser water isotope analyzer in cold and dry polar regions, Atmospheric Measurement Techniques, 14, 2907–2918, https://doi.org/10.5194/amt-14-2907-2021, https://amt.copernicus.org/articles/14/2907/2021/, 2021.

Mahrt, L.: Stably Stratified Atmospheric Boundary Layers, Annual Review of Fluid Mechanics, 46, 23–45, https://doi.org/10.1146/annurev-fluid-010313-141354, https://www.annualreviews.org/doi/10.1146/annurev-fluid-010313-141354, 2014.

Massman, W. J. and Ibrom, A.: Attenuation of concentration fluctuations of water vapor and other trace gases in turbulent tube flow, Atmospheric Chemistry and Physics, 8, 6245–6259, https://doi.org/10.5194/acp-8-6245-2008, https://acp.copernicus.org/articles/8/6245/2008/, 2008.

Munksgaard, N. C., Wurster, C. M., and Bird, M. I.: Continuous analysis of $\delta$ 18O and $\delta$D values of water by diffusion sampling cavity ring-down spectrometry: A novel sampling device for unattended field monitoring of precipitation, ground and surface waters, Rapid Communications in Mass Spectrometry, 25, 3706–3712, https://doi.org/10.1002/rcm.5282, 2011.

Munksgaard, N. C., Wurster, C. M., Bass, A., Zagorskis, I., and Bird, M. I.: First continuous shipboard $\delta$ 18O and $\delta$D measurements in sea water by diffusion sampling-cavity ring-down spectrometry, Environmental Chemistry Letters, 10, 301–307, https://doi.org/10.1007/s10311-012-0371-5, 2012.

Noone, D.: Pairing Measurements of the Water Vapor Isotope Ratio with Humidity to Deduce Atmospheric Moistening and Dehydration in the Tropical Midtroposphere, Journal of Climate, 25, 4476–4494, https://doi.org/10.1175/JCLI-D-11-00582.1, 2012.

Papritz, L. and Spengler, T.: A Lagrangian Climatology of Wintertime Cold Air Outbreaks in the Irminger and Nordic Seas and Their Role in Shaping Air–Sea Heat Fluxes, Journal of Climate, 30, 2717–2737, https://doi.org/10.1175/JCLI-D-16-0605.1, http://journals.ametsoc.org/doi/10.1175/JCLI-D-16-0605.1, 2017.

Peters, L. I. and Yakir, D.: A rapid method for the sampling of atmospheric water vapour for isotopic analysis, Rapid Communications in Mass Spectrometry, 24, 103–108, https://doi.org/10.1002/rcm.4359, http://doi.wiley.com/10.1002/rcm.4359, 2010.

Picarro Inc.: L2140-i, L2130-i or L2120-i Analyzer and Peripherals: Operation, Maintenance, and Troubleshooting User's Manual - 40035, 2013.

Picarro Inc.: L2130-i Analyzer Datasheet, 2021.

Ritter, F., Steen-Larsen, H. C., Werner, M., Masson-Delmotte, V., Orsi, A., Behrens, M., Birnbaum, G., Freitag, J., Risi, C., and Kipfstuhl, S.: Isotopic exchange on the diurnal scale between near-surface snow and lower atmospheric water vapor at Kohnen station, East Antarctica, The Cryosphere, 10, 1647–1663, https://doi.org/10.5194/tc-10-1647-2016, https://tc.copernicus.org/articles/10/1647/2016/, 2016.

Schulz, A.: Untersuchung der Wechselwirkung synoptisch-skaliger mit orographisch bedingten Prozessen in der arktischen Grenzschicht über Spitzbergen, Monograph, Universität Potsdam, https://publishup.uni-potsdam.de/frontdoor/index/index/docId/40005, 2017.

Sodemann, H.: ISotopic Links to Atmospheric water's Sources (ISLAS): [Part B2] ERC Consolidator Grant 2017 Research proposal, 2017.

Sodemann, H., Aemisegger, F., Pfahl, S., Bitter, M., Corsmeier, U., Feuerle, T., Graf, P., Hankers, R., Hsiao, G., Schulz, H., Wieser, A., and Wernli, H.: The stable isotopic composition of water vapour above Corsica during the HyMeX SOP1 campaign: Insight into vertical mixing processes from lower-tropospheric survey flights, Atmospheric Chemistry and Physics, 17, 6125–6151, https://doi.org/10.5194/acp-17-6125-2017, 2017.

Steen-Larsen, H. C., Johnsen, S. J., Masson-Delmotte, V., Stenni, B., Risi, C., Sodemann, H., Balslev-Clausen, D., Blunier, T., Dahl-Jensen, D., Ellehøj, M. D., Falourd, S., Grindsted, A., Gkinis, V., Jouzel, J., Popp, T., Sheldon, S., Simonsen, S. B., Sjolte, J., Steffensen, J. P., Sperlich, P., Sveinbjörnsdóttir, A. E., Vinther, B. M., and White, J. W.: Continuous monitoring of summer surface water vapor isotopic composition above the Greenland Ice Sheet, Atmospheric Chemistry and Physics, 13, 4815–4828, https://doi.org/10.5194/acp-13-4815-2013, 2013.

Steen-Larsen, H. C., Masson-Delmotte, V., Hirabayashi, M., Winkler, R., Satow, K., Prié, F., Bayou, N., Brun, E., Cuffey, K. M., Dahl-Jensen, D., Dumont, M., Guillevic, M., Kipfstuhl, S., Landais, A., Popp, T., Risi, C., Steffen, K., Stenni, B., and Sveinbjörnsdottír, A. E.: What controls the isotopic composition of Greenland surface snow?, Climate of the Past, 10, 377–392, https://doi.org/10.5194/cp-10-377-2014, https://cp.copernicus.org/articles/10/377/2014/, 2014a.

Steen-Larsen, H. C., Sveinbjörnsdottir, A. E., Peters, A. J., Masson-Delmotte, V., Guishard, M. P., Hsiao, G., Jouzel, J., Noone, D., Warren, J. K., and White, J. W. C.: Climatic controls on water vapor deuterium excess in the marine boundary layer of the North Atlantic based on 500 days of in situ, continuous measurements, Atmospheric Chemistry and Physics, 14, 7741–7756, https://doi.org/10.5194/acp-14-7741-2014, https://acp.copernicus.org/articles/14/7741/2014/, 2014b.

Steig, E. J., Gkinis, V., Schauer, A. J., Schoenemann, S. W., Samek, K., Hoffnagle, J., Dennis, K. J., and Tan, S. M.: Calibrated high-precision 17O-excess measurements using cavity ring-down spectroscopy with laser-current-tuned cavity resonance, Atmospheric Measurement Techniques, 7, 2421–2435, https://doi.org/10.5194/amt-7-2421-2014, 2014.

Thurnherr, I., Hartmuth, K., Jansing, L., Gehring, J., Boettcher, M., Gorodetskaya, I., Werner, M., Wernli, H., and Aemisegger, F.: The role of air–sea fluxes for the water vapour isotope signals in the cold and warm sectors of extratropical cyclones over the Southern Ocean, Weather and Climate Dynamics, 2, 331–357, https://doi.org/10.5194/wcd-2-331-2021, https://wcd.copernicus.org/articles/2/331/2021/, 2021.

Wahl, S., Steen-Larsen, H. C., Reuder, J., and Hörhold, M.: Quantifying the Stable Water Isotopologue Exchange Between the Snow Surface and Lower Atmosphere by Direct Flux Measurements, Journal of Geophysical Research: Atmospheres, 126, 1–24, https://doi.org/10.1029/2020JD034400, https://onlinelibrary.wiley.com/doi/10.1029/2020JD034400, 2021.

Weng, Y., Touzeau, A., and Sodemann, H.: Correcting the impact of the isotope composition on the mixing ratio dependency of water vapour isotope measurements with cavity ring-down spectrometers, Atmospheric Measurement Techniques, 13, 3167–3190, https://doi.org/10.5194/amt-13-3167-2020, https://amt.copernicus.org/articles/13/3167/2020/, 2020.

Zeeman, M. J., Selker, J. S., and Thomas, C. K.: Near-Surface Motion in the Nocturnal, Stable Boundary Layer Observed with Fibre-Optic Distributed Temperature Sensing, Boundary-Layer Meteorology, 154, 189–205, https://doi.org/10.1007/s10546-014-9972-9, http://link.springer.com/10.1007/s10546-014-9972-9, 2015.